Historic bar and channel dynamics of the Manukau Harbour entrance

A report prepared by Associate Professor Murray Ford for Tonkin and Taylor Limited.

Date	Version	Description	Prepared by	Reviewed by
08/06/23	01	Draft 01	Murray Ford	Tom Shand
16/08/23	02	Draft 02	Murray Ford	Tom Shand
31/01/24	03	Final	Murray Ford	Tom Shand

CONTENTS

1 EXECUTIVE SUMMARY

The entrance of the Manukau Harbour is a complex geomorphic feature known as an ebb-tidal delta (ETD). The Manukau ebb-tidal delta (METD) is the second largest ETD complex in New Zealand, second only in size to the (ETD) at the entrance to the Kaipara Harbour. The complex array of channels and bars and their ever-changing movement makes the METD both a challenge for safe vessel navigation and a difficult system to understand from a geomorphic perspective. The dynamic nature of the channels and bars are frequently noted but have rarely been described within scientific studies. Using a combination of historic navigation charts and hydrographic survey data from 1862-2023 and optical satellite imagery from 1999-2022, this study examines the changes to the METD since 1862. Results reveal the behaviour of the METD closely conforms to the model of *Ebb-tidal delta breaching* and *Outer delta breaching* processes as suggested in a widely used conceptual model produced by FitzGerald et al. (2000). This process involves a cycle of channel migration, abandonment and new channel formation that has been observed in the satellite record and demonstrated in similar settings using numerical models. Of note, the inner section of the channel, the first ~2.0 km seaward of Paratūtai Island (aka Paratutae Island), shows relative stability as observed in numerical models, while the outer section of the channel is highly dynamic. This cycle of morphological adjustment of the channels and bars at the entrance to the Manukau Harbour appears to have taken place several times since 1862 with the sequence of satellite images since 1999 clearly showing a near-complete phase of this cycle.

2 INTRODUCTION

2.1 Ebb-tidal deltas

In their 1930 book *Legends of the Maori*, Sir Pomare and Cowan cited a proverb: “Kei te tua o Manukau, te kite ki muri ki te Kupenga-o-Taramainuku” (“When you pass out beyond the Manukau waters, do not look back until you reach—or pass—the ‘Fishing-net of Tara’”). Similarly, two Kaumatua of the Ngati-Mahuta Hapū described the loss of an island off the Manukau Harbour which was, according to one Kaumatua, “Kua kai e te tai” (“It was eaten up by the sea”). This Mātauranga illustrates the dynamic nature of the ebb-tidal delta at the entrance of the Manukau Harbour and highlights the two key challenges this system poses for a) safe navigation of vessels transiting the harbour and b) understanding the complex, dynamic geomorphic system.

Ebb-tidal deltas (ETD) are sedimentary accumulations located in front of tidal inlets, resulting from the interplay between tidal and wave-induced currents (FitzGerald, 1984) (Figure 1). Within coastal systems, these deltas hold crucial morphological importance due to several factors. Firstly, they serve as vast sand reservoirs. Secondly, the presence of sand shoals connected with ebb-tidal deltas diminishes the energy of waves reaching the adjacent shorelines. Thirdly, these deltas influence the process of sediment bypass towards the down-drift coastlines, thereby exerting an impact on coastal changes. Lastly, their shallow water and dynamic sandbars make them a prominent hazard to shipping activities.

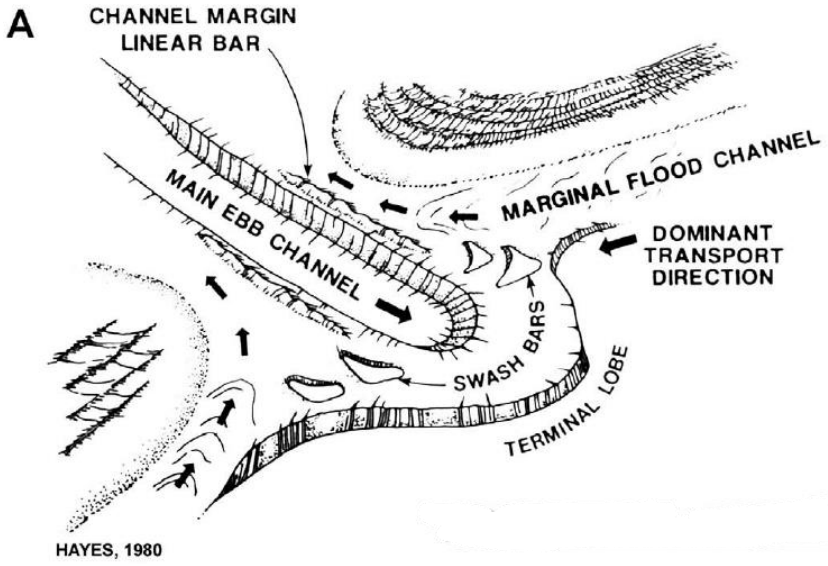

Figure 1. General morphology of ebb-tidal deltas in mesotidal settings (Hayes and FitzGerald, 2013, after Hayes, 1980).

Ebb-tidal deltas serve as substantial reservoirs of sand, holding immense quantities of sediment. Notable examples of large ETD are located on the west coast of the North Island, where the volume of sediment contained within the Kaipara system has been estimated at 12 km^3 and the Manukau 1.25 km^3 (Hicks and Hume, 1996). The sediment within ETD systems can undergo continuous bypass or be periodically released in cycles, effectively influencing, and regulating coastal changes along the adjacent downdrift beaches (FitzGerald, 1984).

Ebb-tidal deltas exhibit distinctive characteristics, including an outward extension of predominantly sand-sized material intersected by the primary channel (FitzGerald et al., 2000). These systems often encompass additional features, such as highly mobile sandbars and secondary channels that tend to be transient in nature (Harrison et al., 2017). The morphology of ebb-tidal deltas is predominantly influenced by the tidal prism, which has been observed to correlate with the sediment volume contained within the delta and wave energy (Walton Jr and Adams, 1976; Hicks and Hume, 1996). Furthermore, various factors, such as wave and tidal flows, sediment supply, local geology, and anthropogenic modifications, such as harbour mouth engineering or disruption of sediment sources, exert control over the morphology and dynamics of ebb-tidal deltas (FitzGerald et al., 2000).

2.2 Objectives

The aim of this study is to describe the dynamics of the Manukau ebb-tidal delta complex over the past 160 years. Three methods are employed to elucidate the behaviour of the Manukau ebb-tidal delta complex (METD). Specific aims of the study include:

- Mapping changes of the METD using historic charts and survey data (1862-2018).
- Mapping the dynamics of the METD using optical satellite imagery from Landsat and Sentinel 2 satellites (1999-2022).
- Analysis of the Ports of Auckland bathymetric datasets to examine changes on the bars and channels with the METD

3 METHODS

3.1 Historic charts and sounding sheets

There have been several nautical charts produced for the entrance to the Manukau Harbour (Figure 2). These charts, and the survey data (sounding sheets) from which they are produced provide the only long-term record of the morphology of the Manukau ebb-tidal delta (METD). The earliest chart accessed was the "Drury Chart" surveyed in 1853 and has been updated several times (Figure 2A and 2B). One version of the chart accessed was updated in 1862 (Figure 2A). Another version of the 1853 chart which was accessed was published in 1937, with "the entrance corrected from Auckland Harbour Board 1919" (Figure 2B). For the purposes of mapping the dynamics of the METD this chart is considered the 1919 chart. The 1862 chart was purchased as a digital download from raremaps.com and the 1919 chart was photographed at the University of Auckland library. All sounding sheets used were provided by the LINZ Hydrographic Office. The 1862 and 1919 charts were georeferenced using likely stable features such as prominent topographic features (rocks, points etc) or navigation beacons.

Interpreting the charts and sounding sheets is challenging as in many cases the charts are a patchwork, pieced together from surveys often spanning several decades. For example, in places the 1962 chart utilises soundings from the 1853 chart. Similarly, even the relatively modern 1992 chart is sourced from surveys conducted between 1960 and 1989. Given the dynamic nature of the bars and channels many of these charts reflect the general morphology of the METD, rather than the morphology of the METD at a point in time. The charts do, however, provide useful updates in places and include additional navigation details and notes.

The raw data that is used in the production of the charts is often available as sounding sheets. The sounding sheets provide data from a narrower date range, typically given as a month, or range of months over which the surveys were undertaken. The sounding sheets which were provided by LINZ are maps with spot depths, with contours and features such as the bars often drawn by the surveyors. It is rare that surveys covered the shallow bars and as a result these features are generally marked on the sounding sheets and charts as "invariably breaks", "continually breaking" or "unsurveyed". The boundary of the unsurveyed areas is the only indication of the position of the bars during the surveys but does not provide a depth over the bars. Consequently, the mapping of the bars itself should be used cautiously. In most surveys the bar is inferred based on the areas that were not surveyed, rather than a precise delineation of the bar itself. The area identified on charts and survey sheets is likely a function of a combination of the position of the bar, the conditions during the survey and the vessel used. It is unlikely that the bar has been identified consistently through time within sounding sheets and on charts. The historic data from

the charts and sounding sheets provides only a general indication of the size and orientation of the bar. In contrast, the channel positions can be more reliably identified from the surveys and charts as the channels are interpreted based on measured depths.

The contours and positions of the shoreline and bars, when mapped, were digitised and stored as shapefiles. The 10 m contour is contour mapped on most sounding sheets and used to compare channel positions. Soundings from the 1862 and 1919 chart are sparse which limits the ability to generate contours. Of note, earlier sounding sheets were surveyed in fathoms, with the 6-fathom contour (10.97 m) used in place of the 10 m contour.

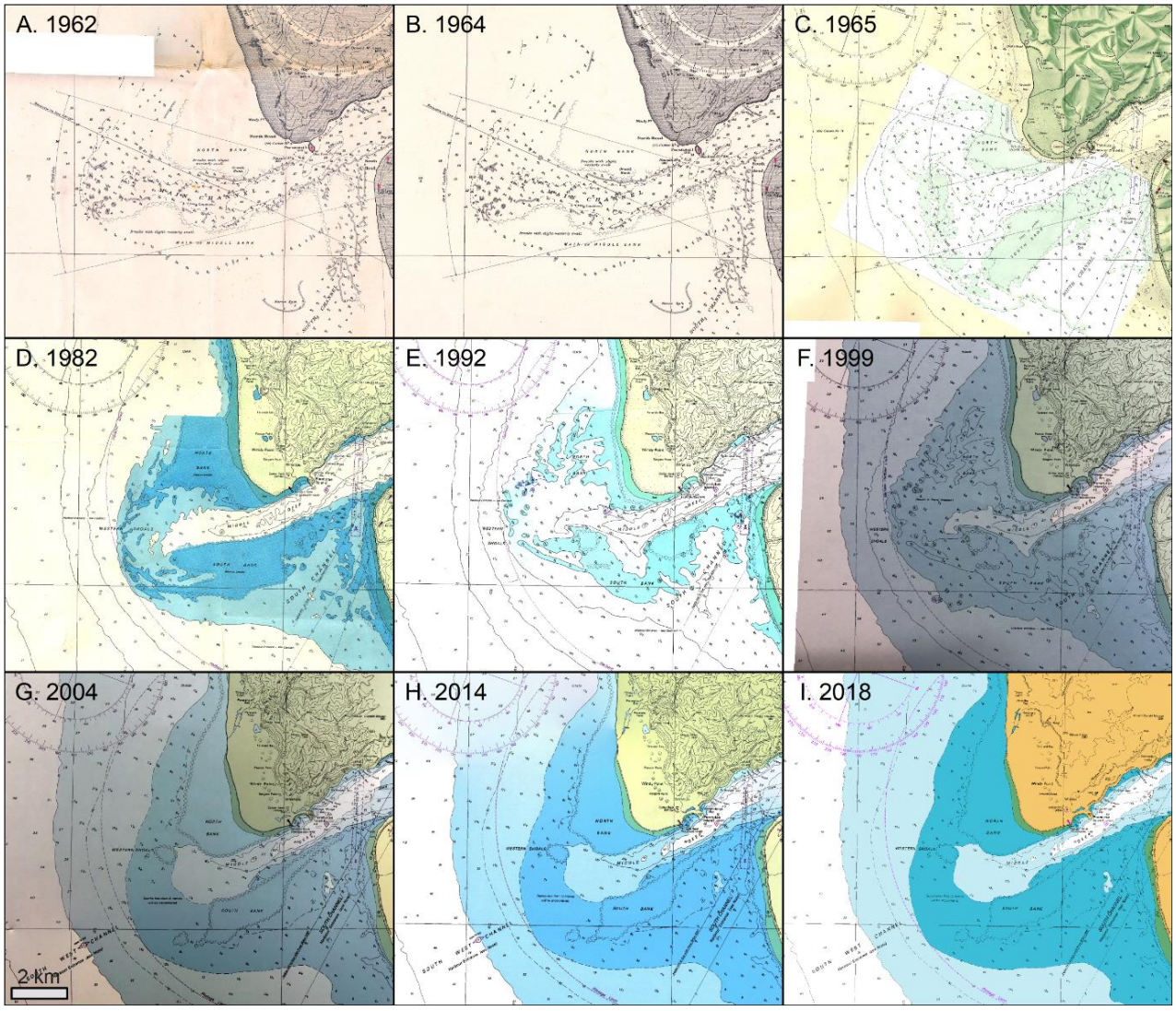

Figure 2. Historic versions of the NZ4314 chart of the Manukau Harbour entrance

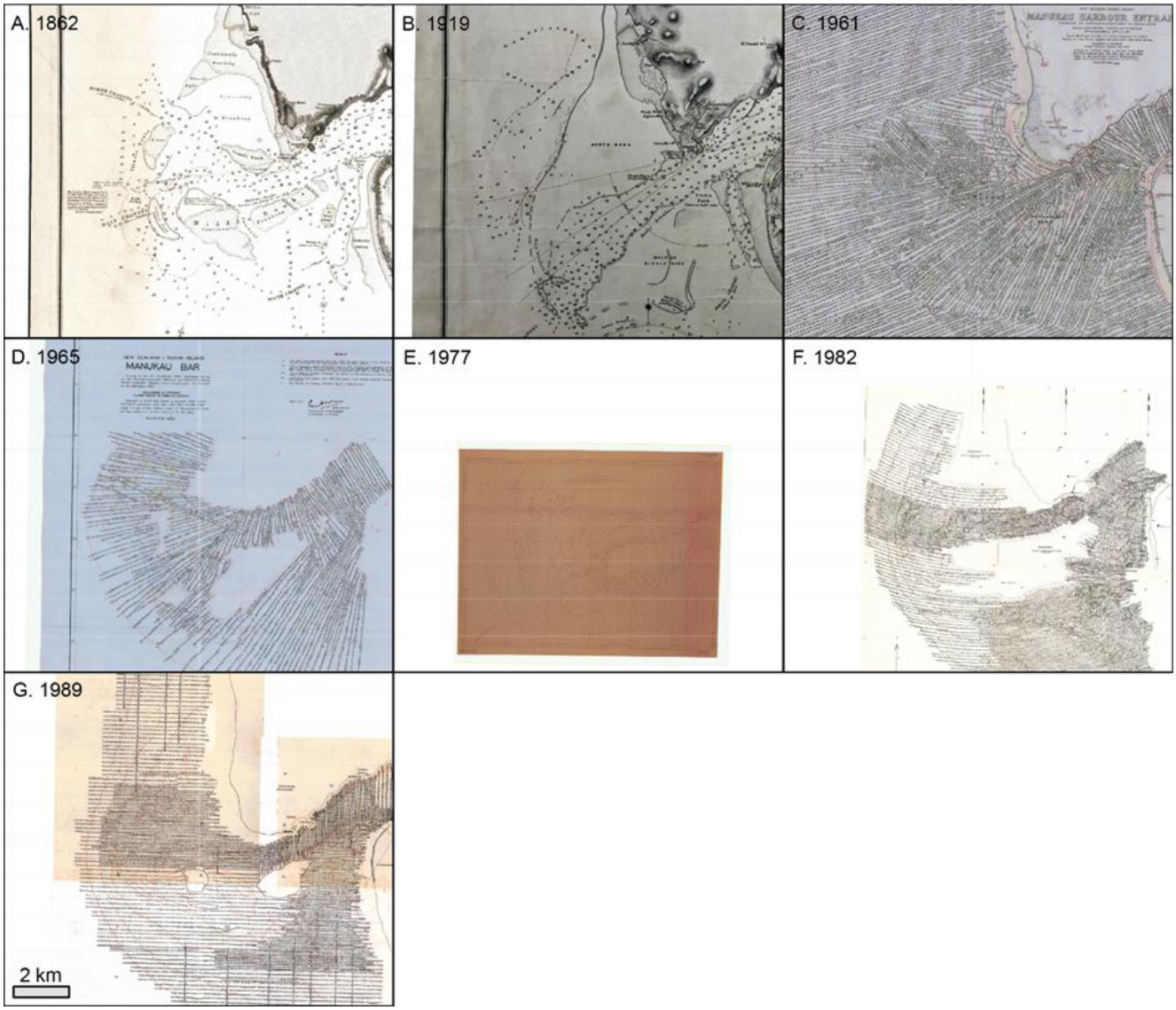

Figure 3. Scans of historic charts and sounding sheets of the Manukau Harbour entrance. Source: Raremaps.com (A), University of Auckland library (B), LINZ (C-G)

3.2 Gridded bathymetry (1989 and 2023)

To estimate the style and volumes of change of the METD system two digital elevation models (DEM) were generated. A 1989 DEM was created by MetOcean by digitising the 1989 sounding sheet and creating x,y,z points from scanned sounding sheets. Additional points, generally from deep water, were added to the 1989 features from the 1961 sounding sheet to expand the coverage of data into beyond the seaward extent of the terminal lobe of the METD. These data were then gridded to a 10 m resolution to provide a seamless DEM of the METD and surrounding areas. Similarly, the 2023 hydrographic survey undertaken by DML were delivered in a 10 m gridded format. To compare bed level changes and estimate deposition and erosion of sediment both DEM's were clipped to a common extent, which is 85.89 km^2. Two pieces of analysis were conducted to compare changes between the 1989 and 2023 DEM's. Firstly, the difference between the 2023 and 1989 DEM's was calculated by subtracting the 1989 DEM from the 2023 DEM for each 10 m pixel within the DEM. Second, estimates of the cut (erosion) and fill (deposition) volumes were calculated providing a planform area of cut and fill, along with the associated volumes of cut and fill.

3.3 Ports of Auckland Surveys

The Ports of Auckland (POAL) surveyed the entrance to the Manukau Harbour and provided data from 2001-2016. The frequency of surveys varied through time, but in some years there were up to five surveys. The POAL surveys have ceased as the Port of Onehunga closed in 2016 and visits of large ships have largely ended. Surveys by the POAL were conducted with Single Beam Echosounder (SBES). The surveys were designed to determine the safest routes out of the harbour for shipping, rather than map the entire METD complex like the 1862-1989 surveys. Consequently, the data were generally captured as transect lines through the likely safest transit along the main channel and across the bar at the terminal lobe. Surveys were generally repeated along the same transects, with most transects generally oriented parallel to the channel, with four cross-channel transects regularly resurveyed. (Figure 4 and appendices 4 and 5).

Data was delivered as eastings, northings and depths recorded in the Mt Eden Circuit coordinate system (earlier files were in the 1949 Mt Eden Circuit, with more recent files in the 2000 Mt Eden circuit) and stored as text files. Files were loaded into ArcGIS, converted to New Zealand Transverse Mercator 2000 (NZTM2000) coordinate systems, and stored as shapefiles.

The POAL surveys include data from the transit through the main, and sometimes south, channel to the primary survey area across the main bar (Figure 4A). The data was 'cleaned' to produce two versions of the survey data. Firstly, to enable gridding of the point data, the portion of the surveys that included transit

data was removed to create a dense collection of points within a confined neighbourhood (Figure 4B). Secondly, an additional version of the data was produced that only contained data within 20 m of the transects. Each transect was then assigned a unique identifier (Appendix 4).

There are numerous methods to grid SBES stored as points. EL-Hattab (2014) published extensive trials of different methods to rasterise SBES data and found a two-step process involving creating a Triangulated Irregular Network (TIN) from the point data and then rasterising the TIN produced the lowest errors. Following this method, a TIN was generated from the POAL data and then converted to a Geotiff within a 10m resolution.

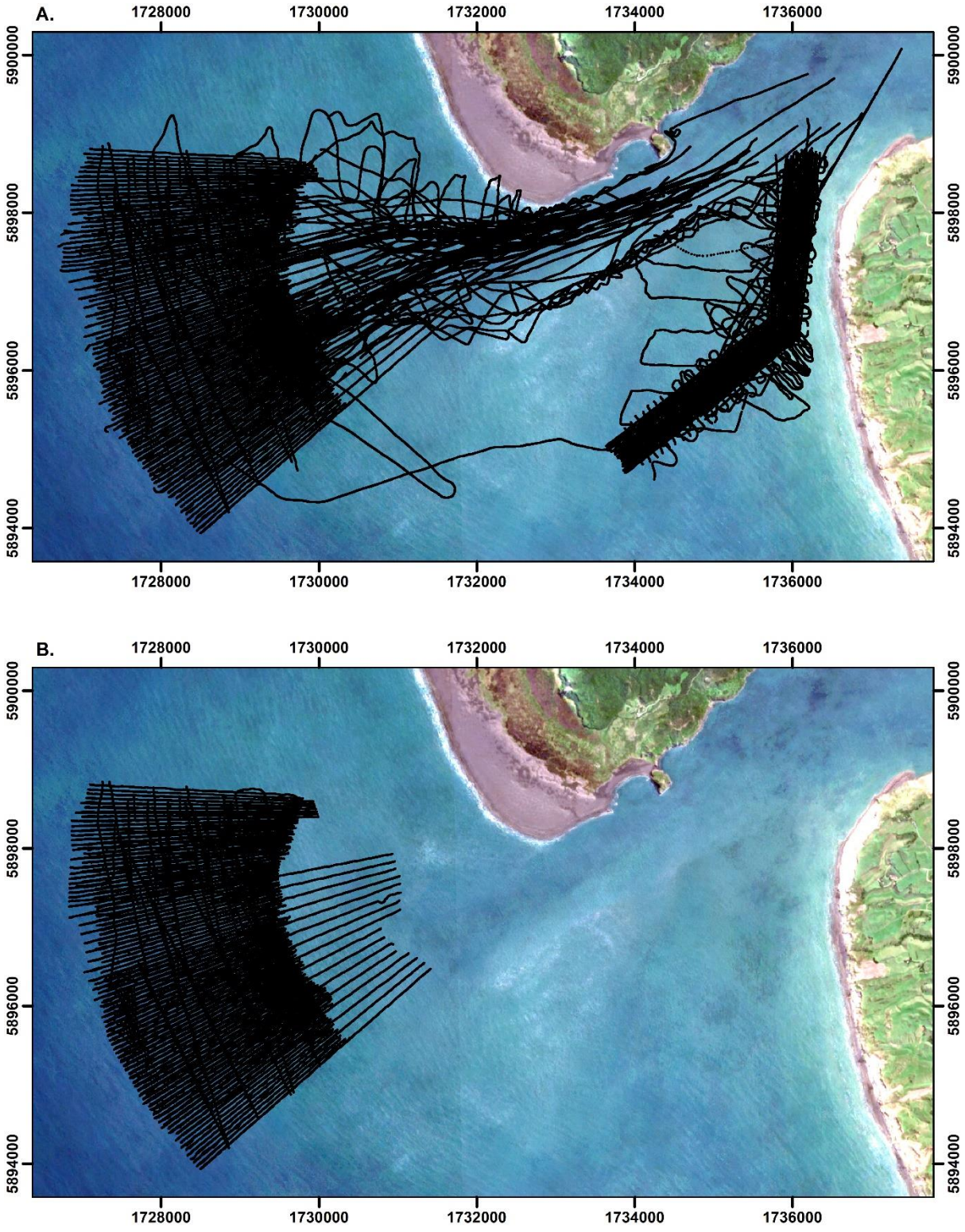

Figure 4. A). All POAL SBES survey data. B) Subset for POAL SBES data used in the creation of 10 m resolution grids.

3.4 Satellite detection of ebb-tidal delta dynamics

Remote sensing studies of ebb-tidal deltas (ETD) have typically utilised imagery from ground-based, airborne and spaceborne sensors to successfully examine ETD dynamics. Ground-based cameras, such as those within the Argus or the Cam-Era systems, have been widely used to examine nearshore processes including rip detection, ETD dynamics and bar migration based on the contrast between broken (bright) and unbroken waves (dark) in digital images (Figure 5). When stacks of images are time-averaged, areas of persistent broken and unbroken water become increasingly evident. Such techniques are often used to indicate the presence of rips where wave breaking is relatively low compared to areas adjacent to the rip channel, resulting in time-averaged pixels which appear dark in a greyscale image. Conversely, shallow water over bars forces wave breaking resulting in highly reflective surface which appears white in a greyscale image.

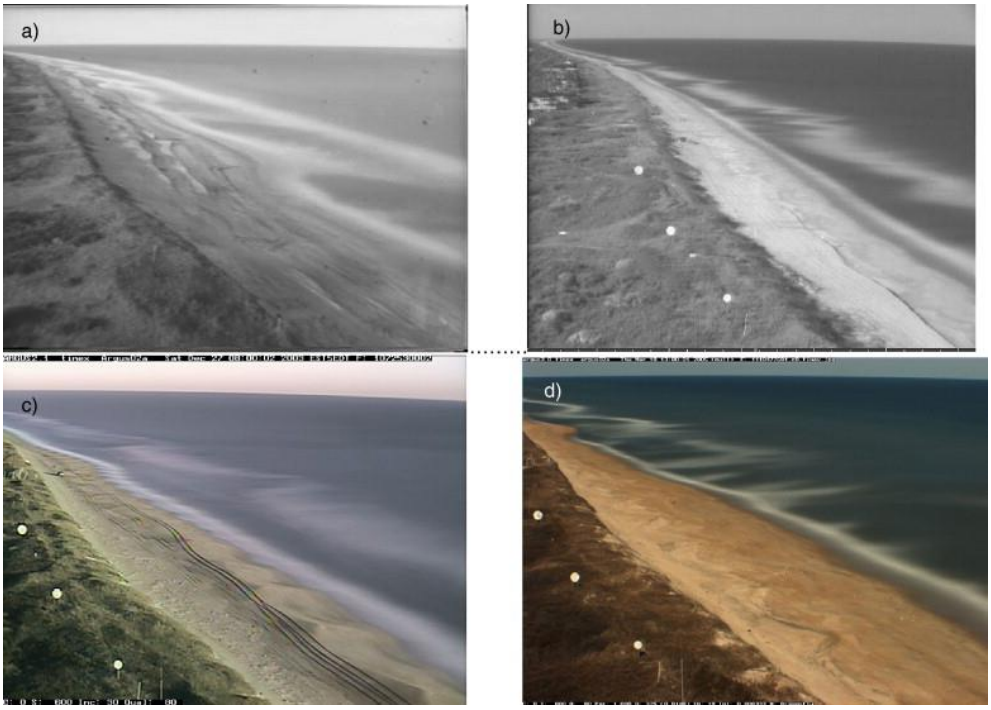

Figure 5. Example of time-averaged imagery from ground-mounted cameras. Time-averaging of image stacks reveals bars/channels and other morphological features. Source: Holman and Stanley (2007)

Recently, the time-averaging techniques used on ground-mounted cameras have been adapted for satellite imagery and applied at ETDs (Figure 6). Ford and Dickson (2018) time-averaged imagery captured by the Landsat 7 and 8 satellites of the Manukau Harbour ETD on the west coast of Auckland, New Zealand and were able to observe migration of the bars and channels of >1 km on decadal timescales. Both Landsat 7 and 8 capture 15-30 m resolution imagery of the same location every 16 days, or 8 days in locations where orbital paths overlap.

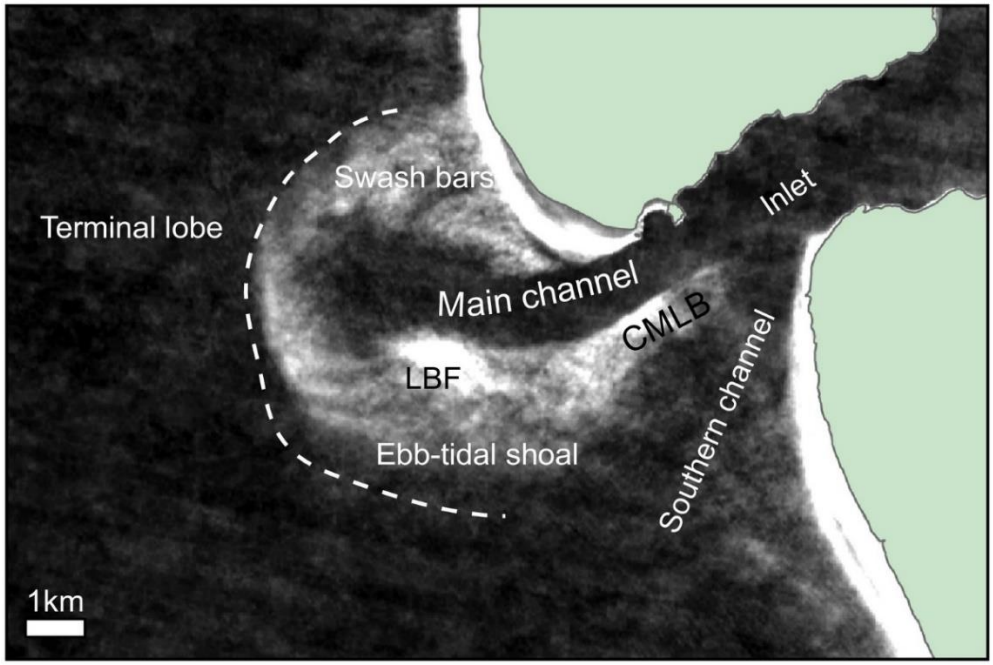

Figure 6. Time-averaged collection of Landsat 7 and Landsat 8 imagery covering the Manukau ETD used to identify common geomorphic features of ebb-tidal deltas CMLB = Channel margin linear bar. LBF = Linear bar formation. Source: Ford and Dickson (2018)

3.4.1 Analytical steps

In order to produce time-averaged images from optical satellite imagery a number of steps in data processing and analysis were undertaken within Google Earth Engine, before outputs (geotiffs) were exported for use within a desktop GIS. The analytical steps are summarised in Figure 7.

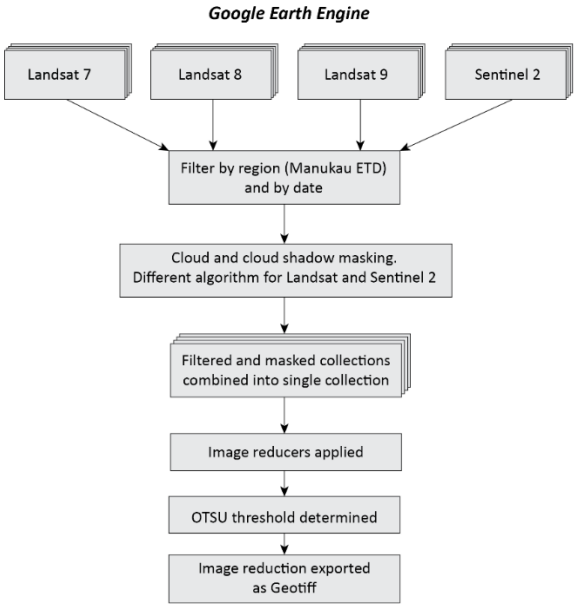

Figure 7. Analytical steps applied to determine the bar positions at the Manukau ebb-tidal delta.

3.4.2 Imagery

The Landsat program has provided near-continuous observation of the Earth's surface since 1972 (Figure 8). There have been nine Landsat missions, seven of which successfully reached orbit (Landsat 6 did not reach orbit). Importantly for this study, Landsat 7 carried the Enhanced Thematic Mapper Plus (ETM+) sensor which has eight spectral bands, three in the visible light range (Blue, Green and Red), three in the near and shortwave infrared and one thermal band acquired at 60 m and resampled to 30 m (Markham et al., 2004). Landsat 8 and Landsat 9 has four 30 m spatial resolution bands in the visible light spectrum, ("Ultra-blue", Blue, Green and Red). At present, L8, launched in 2013 and L9, launched in 2021 are operational. In 2003, the L7 sensor suffered a scan line corrector (SLC) fault and since this time has operated at a reduced capability with a ~22% loss of data (Scaramuzza et al., 2004). The SLC fault resulted in low-image availability and low image quality from 2003 until 2013.

The Sentinel-2 mission is a part of the European Space Agency's Copernicus program that aims to provide high-resolution, multi-spectral images of the Earth's land and coastal regions for various applications such as agriculture, forestry, land use and management, and disaster monitoring. The mission is composed of two identical satellites, Sentinel-2A (launched in 2015) and Sentinel-2B (launched 2017), both satellites are equipped with a multi-spectral imaging instrument (MSI) that has 13 spectral bands ranging from visible to shortwave infrared with a spatial resolution of 10, 20, or 60 meters depending on the band. The Sentinel-2 Multi-Spectral Instrument (MSI) has four visible and near-infrared (VNIR) bands, which include the red, green, and blue bands, as well as a near-infrared band. The spatial resolution of these VNIR bands is 10 meters. The Sentinel-2 satellites orbit the Earth in a sun-synchronous polar orbit at an altitude of approximately 786 km, with a revisit time of 5 days at the equator, providing global coverage every 5 days.

We utilised imagery from Landsat 7 (1999-2002), Landsat 8 (2013-2022), Landsat 9 (2021-2022) and Sentinel 2 (2015-2022) in this study.

Figure 8. Timeline of Landsat satellites

3.4.3 Google Earth Engine

Google Earth Engine (GEE) was used to process the collection of Landsat and Sentinel 2 imagery. The GEE is a cloud-based application for geospatial data analysis (Gorelick et al., 2017). GEE provides access to a wide range of remote sensing algorithms which are run on Google's servers, negating the need for high-performance local computing. The GEE has been used to study a wide range of environments and processes in the coastal zone including: shoreline change (Mao et al., 2021), mangroves (Chen et al., 2017), coral reef islands (Holdaway et al., 2021) and ebb-tidal delta dynamics (Ford and Dickson, 2018). Users can access the GEE through a web-based code editor, which we used in this study, or can be accessed via a Python API. Within GEE a stack of imagery is referred to as an image collection. Users can access existing image collections of freely available imagery within GEE (i.e. Landsat, Sentinel-2 and others) or can create their own image collections stored within GEE. Image collections are filtered by date and by area of interest, for example, filtering delivers all imagery which intersects the entrance to the Manukau Harbour within a given year.

3.4.4 Cloud masking

Visually the white, foaming bubbles which result from wave breaking are in stark contrast to the unbroken water which surrounds them. However, visually clouds appear similar to broken water, with similarly high reflectance values in the visual wavelengths of light. Conversely, the shadows cast by clouds can make pixels appear darker. In order to address cloud and shadow contamination all images were cloud-masked, a process through which pre-existing cloud mask layers are applied to each image in order to mask, or exclude, cloud or cloud shadow contaminated images from analysis (Figure 9).

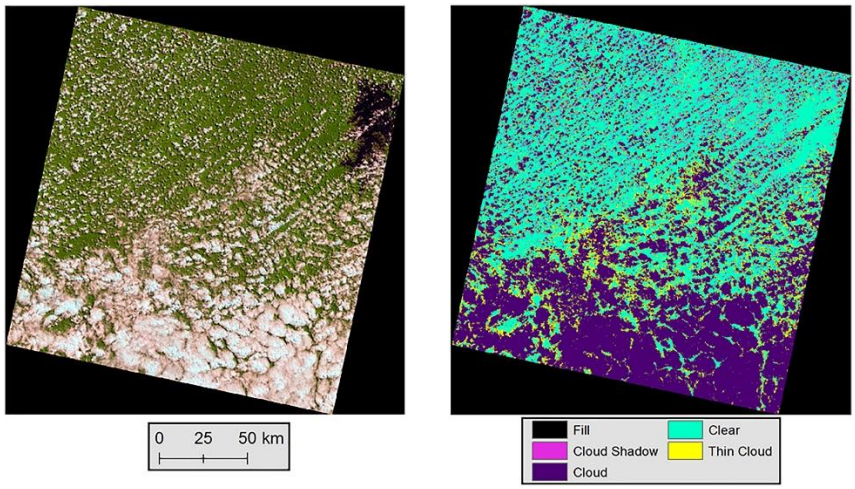

Figure 9. Example of cloud and cloud shadow masking. Only pixels classified as clear are used in the analysis of wave breaking.

3.4.5 Image Collection Statistics

A range of summary statistics can be calculated from an image collection on a per-pixel basis through an image collection. Within GEE these operations are known as image reductions, where a collection of images is reduced to a single output image. An image reduction is essentially deriving a time series at each pixel in the image collection and then calculating statistics from each resulting time series, while excluding cloud and cloud shadow masked pixels (Figure 10). Many of the common image reductions (i.e. mean, median and standard deviation) are analogous to methods applied to stacks of imagery from terrestrial images captured by the likes of Argus or Cam-era systems.

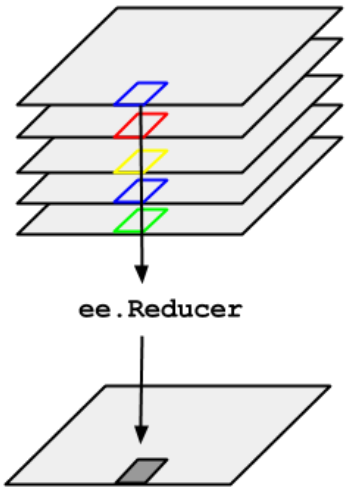

Figure 10. Example of an image reduction. Source: https://developers.google.com/earth-engine/guides/reducers_image_collection

Ford and Dickson (2018) demonstrated that the mean, median and standard deviation values all produce outputs which clearly demarcate the bars and channels on ebb-tidal deltas (Figure 11). However, the median reduction has a tendency to underestimate the extent of the bars, while the mean and standard deviation can be prone to being impacted by any cloud and shadow pixels which weren't detected and masked by the cloud-masking algorithms. As such, we explored the use of the percentile reducer to determine the utility in mapping the METD. Practically, given the stark contrast between highly-reflective broken pixels and unbroken pixels there is only minimal observable difference in the various image reducers. For consistency, the 90th percentile value was adopted as the reducer.

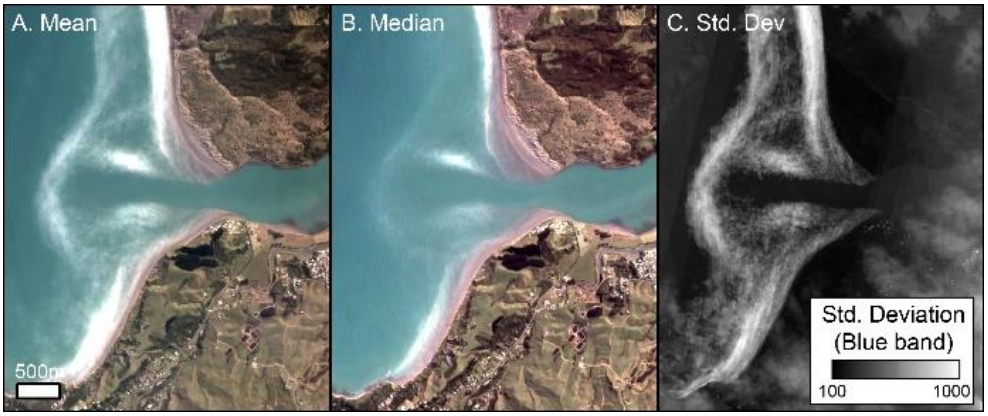

Figure 11. Example of the mean, median and standard deviation reducers applied to collections of optical satellite imagery at the Raglan Bar. Modified from Ford and Dickson (2019).

3.4.6 Wave and water level controls on breaking

To examine tidal and wave controls on breaking, Ford et al. (2021) appended the water level relative to chart datum and incident wave height at the time of image capture as metadata properties to each satellite image of the Raglan Bar. This enabled the collection of images of Raglan to be filtered based on date, water level and wave height. Ford et al. (2021) demonstrated that this approach allowed for the state of the Raglan Bar to be mapped for various combinations of water level and wave height (Figure 12). Ford et al., (2021) were able to map the particular bars upon which wave breaking was forced based on water level and wave height.

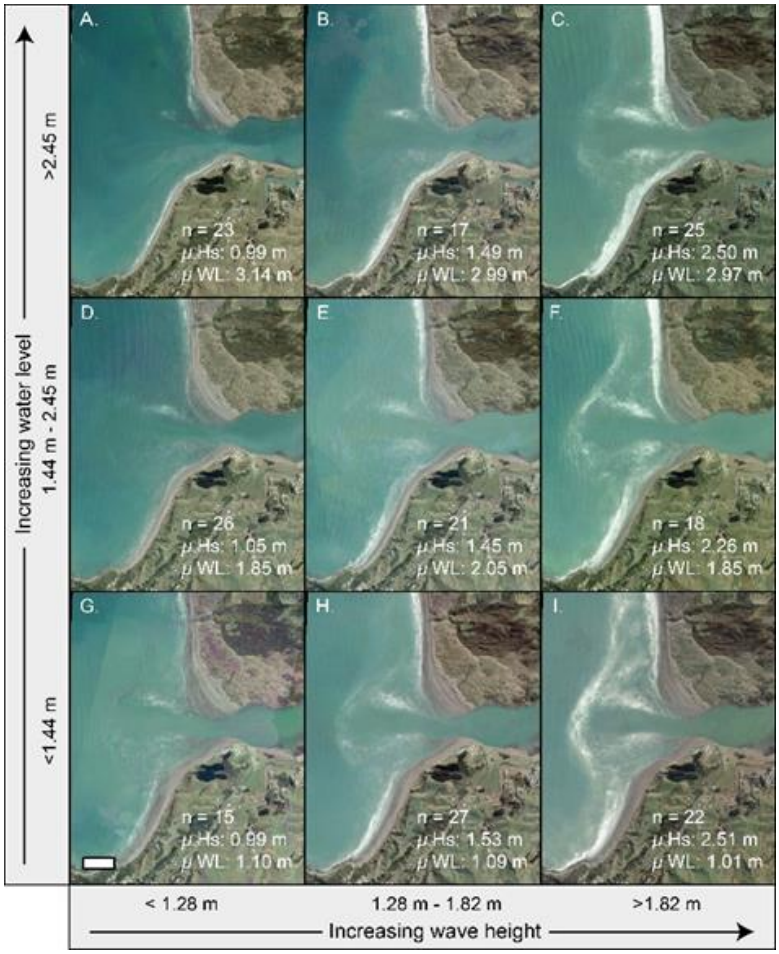

Figure 12. Mean image reductions of collections of commercial PlanetScope TOA imagery of Raglan Harbour from 2017-2019 filtered into the highest, middle and lowest one-third of water levels and wave heights showing patterns and extent of breaking under different conditions. Source: Ford et al. (2021).

Following the approach of Ford et al., (2021), the mean sea level (MSL) and offshore wave height at the time of image capture were added as metadata properties to cloud-free satellite images of the Manukau harbour entrance. To add water level and wave height properties to each image, a new image collection comprised of cloud-free images from Landsat 7-9 and Sentinel 2 satellites was created. This collection was manually generated following the inspection of all images which covered the Manukau Harbour entrance from 1999-2022. All images were loaded within a viewer and visually inspected. Images that were largely unimpacted by cloud and cloud-shadow were retained within the collection, with cloudy images discarded. This approach differs from that adopted in Section 3.3.4, which applied a per-pixel cloud mask. By creating a manually screened image collection the water level and wave height values at the time of image acquisition are applied as per-image metadata properties. All resulting analyses involving wave height and water level were then performed on every pixel in the image collection, without masking, which provides a uniform time-series of pixel values at each pixel. This enables the image collection to be filtered and time-averaged based on date, water level and wave height.

3.4.7 Water level at the time of image acquisition

Water level was calculated using the NIWA tide forecaster (https://niwa.co.nz/information-services/tide-forecaster), which provided a timeseries with 10-min intervals of predicted tidal levels, relative to MSL, from 1999-2022. There is a tide-gauge on Paratūtai Island , which would provide measurements of water level including time-varying components driven by oceanographic and climatic processes. However, this record has several gaps and does not extend back to the Landsat 7-era. For consistency, the predicted water level from the NIWA tide forecaster was adopted. The predicted tide level closest to the time of image acquisition was appended as the water level value.

3.4.8 Wave height at the time of image acquisition

A time series of significant wave height (Hs) ~30 km offshore of the Manukau Harbour was generated from a global wave hindcast. The wave hindcast was produced by the Australian Bureau of Meteorology (BOM) and Commonwealth Scientific and Industrial Research Organisation (CSIRO) using the Wave Watch III (WW3) model run. The WW3 hindcast was run at 0.4 degree resolution. (Durrant et al., 2013). The significant wave height (Hs) value from the model was extracted at 37.2°S and 174°E with hourly time-steps. The WW3 value closest to the time of image capture was appended as an image property. All images within the image collection had a metadata property of water level (WL) and offshore wave height (Hs). Appending the WL and Hs enables the image collection to be filtered based on wave height and wave level.

4 RESULTS

4.1 Satellite observations of channel and bar dynamics

Ford and Dickson (2018) demonstrated that time-averaged collections of optical imagery from the Landsat satellites are effective at mapping the channels and bars at the entrance to the Manukau Harbour. This analysis has been extended to include additional imagery from the Sentinel 2 satellites and the recently launched Landsat 9 satellite. Several geomorphic features commonly observed in the ebb-tidal deltas can be easily identified using the time-averaging analyses. These features may not be easily interpreted from a single image alone. The analysis of time-averaged images enables identification of specific areas where wave-breaking occurs frequently, both near the beach and on offshore sandbars (Figures 13 and 14). Additionally, time-averaging helps in distinguishing unbroken water associated with channels, sheltered sections of the harbour, and deep water. The following features can be identified at the METD: linear bar formation (LBF), channel margin linear bars (CMLB) running parallel to the main channel, swash bars, and the terminal lobe marking the outermost extent of wave breaking (Figure 6). Likewise, with a timeseries of images spanning 1999-2022 it is possible to track the migration of these features at a much higher temporal resolution than would be possible using hydrographic surveys (Figure 13).

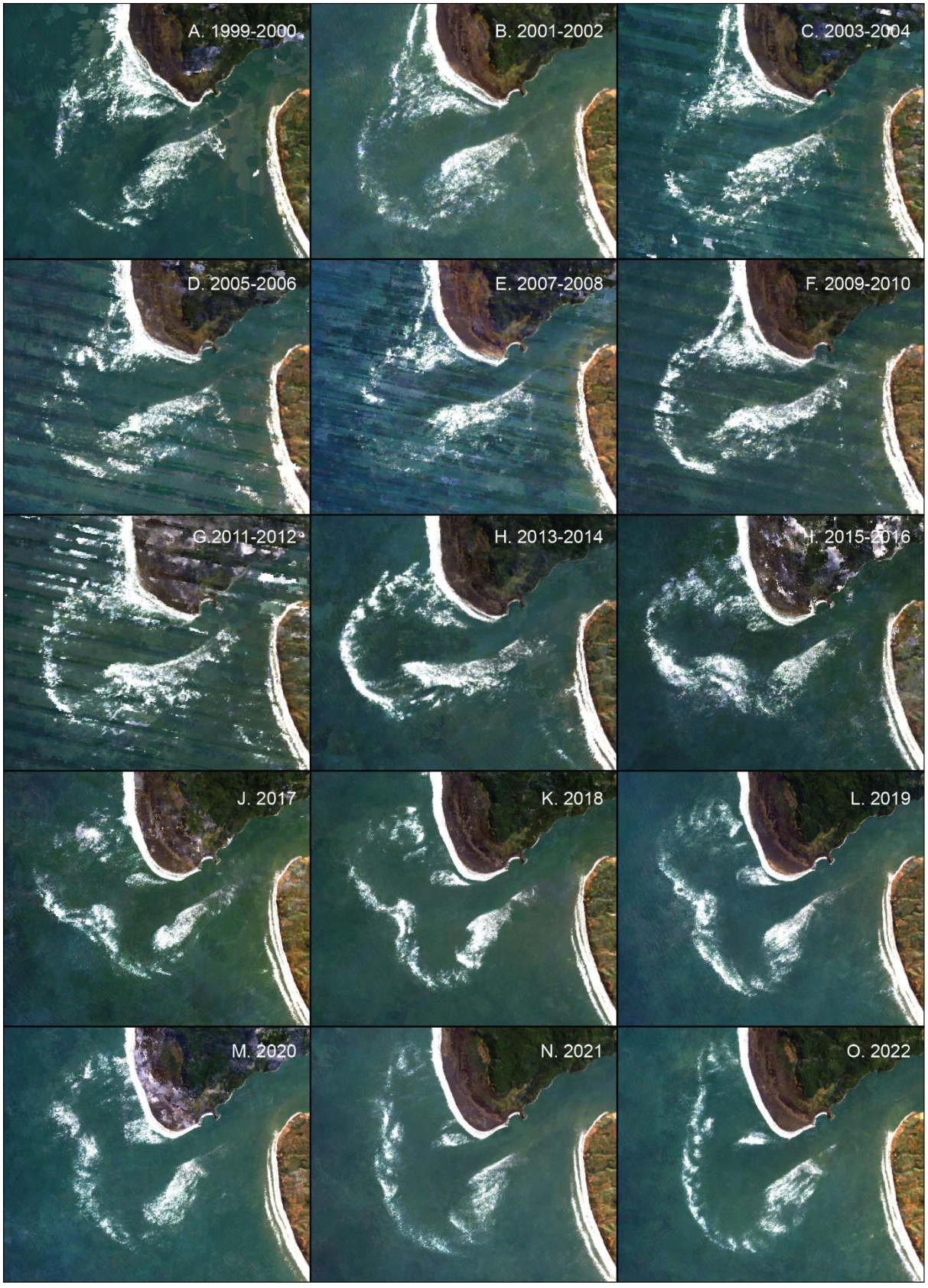

Figure 13. True colour 90th percentile image reductions of Landsat and Sentinel 2 imagery of the METD.

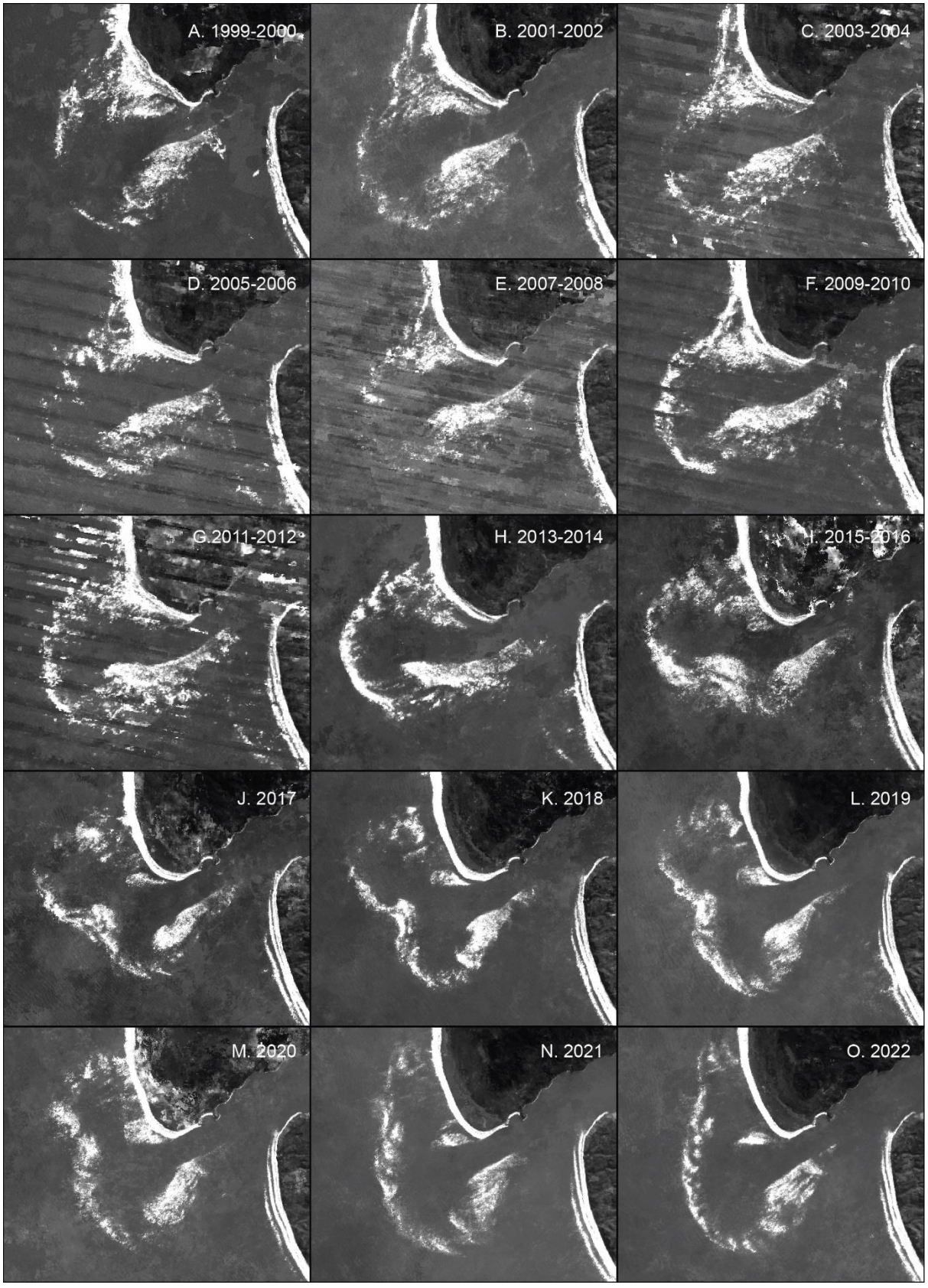

Figure 14. 90th percentile image reductions of the blue band from Landsat and Sentinel 2 imagery of the METD.

Ford and Dickson (2018) observed notable changes in the northern channel's outer sections between the years 2000 and 2002 (when Landsat 7 operated without scanline corrector fault) and the years 2014-2016 (combined Landsat 7 and Landsat 8 collection), with a northward migration of >2 km, a rate of ~140 m/yr. Concurrently, the terminal lobe, where wave breaking is most frequent, shifted offshore. Moreover, wave breaking generally occurred further offshore during the years 2014-2016 compared to 2000-2002. By extending the window of analysis to 2022 and by including imagery from Landsat 9 satellite and the Sentinel 2 satellites, additional detail on the behaviour of the METD can be elucidated than was presented in Ford and Dickson (2018).

Analysis in this study showed that between 1999-2000 and 2022 the METD is characterised by the northward rotation of the channel, reaching a maximum northward extent in the 2015-2016 period. Ford and Dickson (2018) observed the possible emergence of a new southward oriented channel forming through the south bank. The emergence of this channel is confirmed in the 2017-2022 images from this study. The sequence of time-averaged images reveals three distinct behaviours of the METD: the migration of the terminal lobe, the stability of the inner section of the channel and south bank, and the bifurcation of the south bank and formation of a new south-westerly oriented channel .

4.1.1 Migration of the terminal lobe

The terminal lobe is identified from the time-averaged satellite imagery as the most seaward extent of white water caused by wave breaking. It is similar in position and shape as the 10 m contour from bathymetric surveys but is not directly a measure of depth (Figure 15). The terminal lobe was manually identified as the seaward extent of white water in the time-averaged imagery and was digitised (Figure 15). The terminal lobe varied in position by between 1-2 km over the 1999-2022 study period. The maximum seaward distance of the terminal lobe was measured as the maximum distance of the terminal lobe from the centre of the channel near Paratūtai Island (Figure 15). In 1999 the maximum distance was towards the southwest limit of the terminal lobe and stayed approximately in this location until ~2013-2014 when it shifted to the north. The northward migration of the terminal lobe continued until it reached a maximum northern extent in 2019. The maximum distance moved south slightly between 2019 and 2020, before returning to its most southern orientation in 2021.

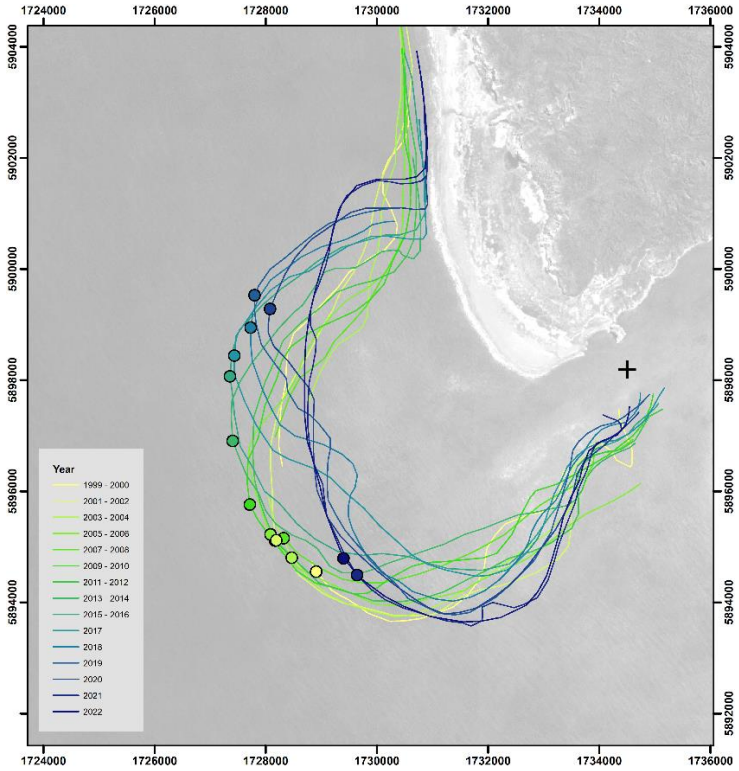

Figure 15. Seaward extent of the terminal lobe of the Manukau ebb-tidal delta interpreted from time-average Landsat and Sentinel 2 images. Points represent the maximum distance of the terminal lobe from the centre of the channel near Paratūtai Island marked by + on the map.

4.1.2 Main channel and bank dynamics

Analysis of satellite imagery from 1999-2022 reveals the position of the southern bank of the channel, which marks the edge of the south bank, is stable for ~2 km seaward from a point aligned with Paratūtai Island (Figure 16). Seaward of this point the position of the south bank shows noteworthy change through time. From ~2009-2010 we observe the northward rotation of the outer section of the south bank, this is particularly evident when in the 2013-2014 image (Figure 13H). Strikingly, the 2015-2016 image shows the beginning of the bifurcation of the south bank and a new southerly oriented channel begins to push through the south bank. The process initiates the formation of the new south-westerly oriented channel. The continued evolution of this channel is evident through until 2019-2022 when the channel appears fully formed. Little change is observed between 2020 and 2022 suggesting the channel has reached a stable morphology, which is not too dissimilar to the morphology of the bar in 1999-2000.

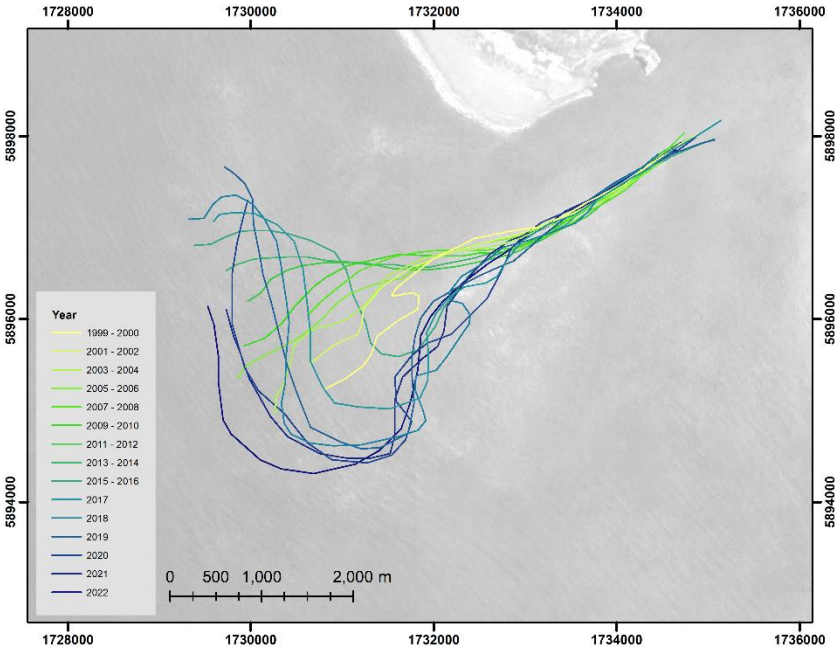

Figure 16. Position of the channel-side boundary of the channel margin linear bar (south bank) of the Manukau ebb-tidal delta interpreted from time-average Landsat and Sentinel 2 images.

4.1.3 Water level and wave conditions during image acquisition

It has been suggested that the collection of satellite images used in these types of analysis may not be fully reflective of the range of conditions on METD (Ford and Dickson, 2018). There is the potential for bias in the image collection with the potential for more images from summer which is generally characterised by lower cloud-cover and lower wave heights. Similarly, the Landsat and Sentinel 2 satellites acquire images in the middle of the morning, local time (approx. 10 am). As a result, depending on the tidal regime these satellites can be biased towards collecting at certain tidal conditions. The average water level at the acquisition time of the cloud-free images was 0.25 m (MSL) (Figure 17). This compared to average predicted water level (1999-2022) of 0.00 m. The average offshore wave height during the cloud-free image acquisition (Hs) was 2.27 m, with a 90th percentile of Hs of 3.47 m and max Hs of 6.20m. The average offshore wave height between Dec-1999 and Dec-2022 was 2.41 m, with a 90th percentile of Hs of 3.76m and max Hs of 9.69m. Figure 18 presents the time-averaged collection of images under different tidal levels and offshore wave heights.

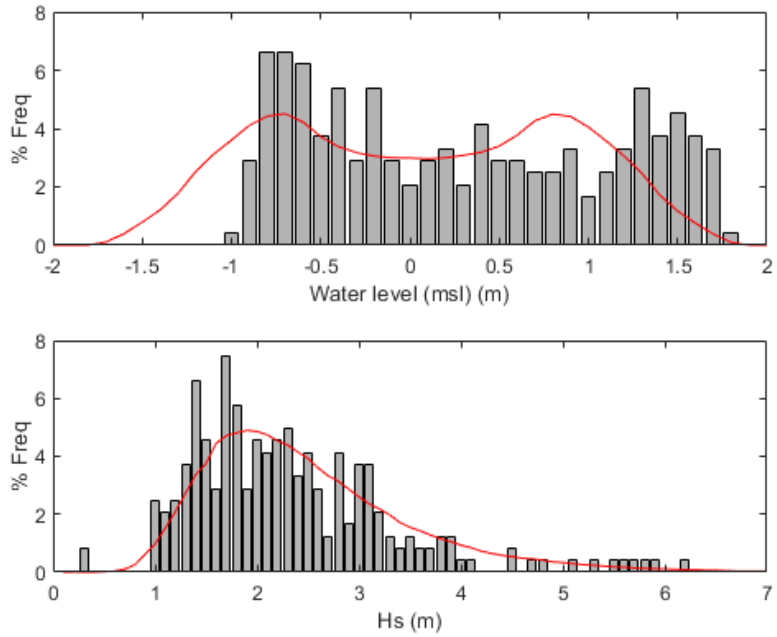

Figure 17. a) Histogram of water level relative to MSL at the time of image acquisition, red line is the distribution of water level predictions from 1999-2022. Date source: NIWA tide predictor. b) Histogram of significant wave height (Hs) values between 1999-2022 from a wave hindcast (WW3 model) run by CSIRO/BOM.

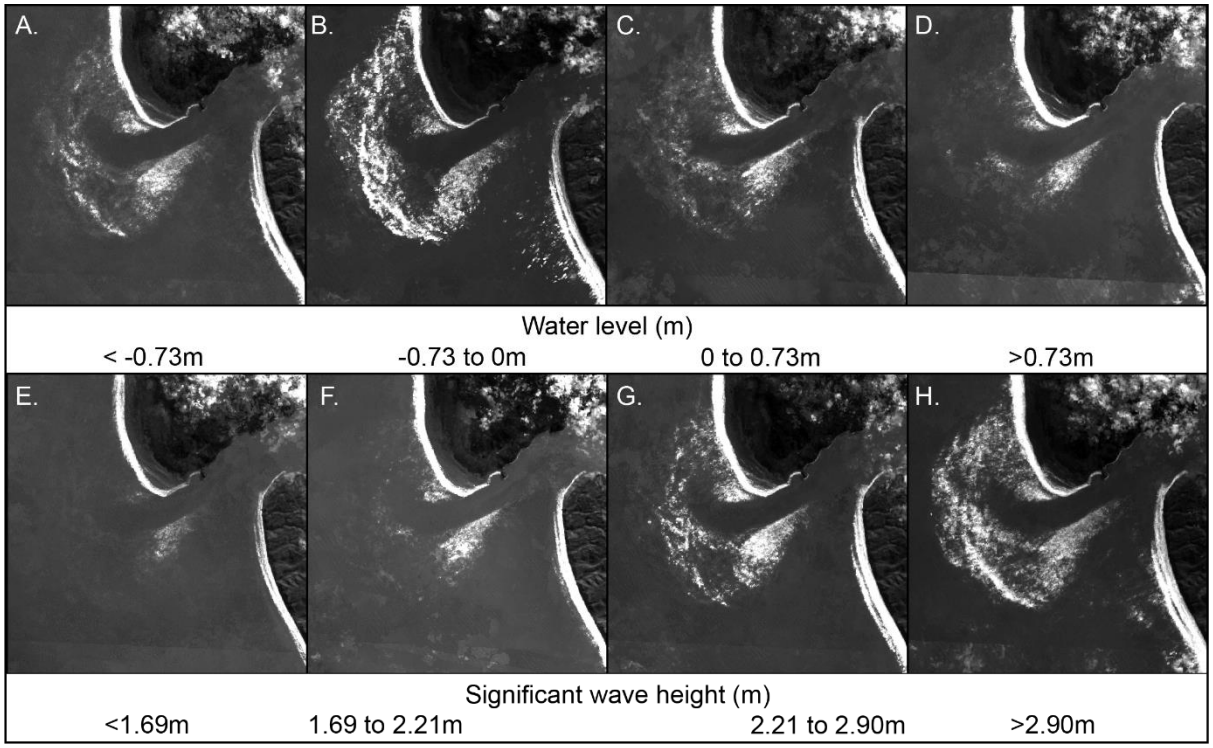

Figure 18. Median image reductions of the blue band from the 1999-2022 Landsat and Sentinel 2 image collection. The image collection is filtered by water level quartiles (panels A-D) and offshore significant wave height (panels E-H).

4.2 Historic surveys and charts of the Manukau Entrance (1862-2023)

Historic surveys of the METD reveal a complex system with many of the common morphological features and behaviours of ebb-tidal deltas. First, there is evidence of the relative stability and persistence of the inner section of the channel margin linear bar (CMLB). Second, the inner section of the channel appears stable and is marked in similar positions in all charts and surveys. Third, the outer section of the channel appears highly dynamic, with the orientation of the outer section of the channel notably different across the time intervals.

4.2.1 Channel and Bar dynamics

In some surveys there are three distinct channels present through the METD. This is particularly evident in the 1862 chart where a north, main and south channel are clearly marked (Figures 3 & 19 and appendix 1). In contrast, the 1919 map shows only the main channel, with the south channel noted as “silted up”. Aside from the 1919 chart, the south channel appears a consistent feature, as does the main channel, which is sometimes (i.e. 2004) referred to as the west channel. The north channel is neither clearly defined, nor regularly labelled on navigation charts. However, the outer section of the main channel is sometimes oriented west-northwest and the bar appears more poorly defined along the northern section (i.e. 1965). The inner section of the main channel appears relatively stable with a consistent west-southwest orientation (~240°). This stable section of the channel extends 2.5-3.0 km offshore from Paratūtai Island. This section of the channel aligns with the area named the “Middle Deep” on the most recent NZ4314 chart. The depth of this stable section is over 30 m over the first ~2 km offshore from Paratūtai Island before gradually shallowing to ~20 m before the channel begins to show evidence of migration. Seaward of the stable throat section of the main channel oscillates from the most southerly orientation as surveyed in 1919 through to more westerly alignment in 1961,1965 and 1992. Of note, the raw soundings from the 1961 surveys show several repeated transects on a northwest oriented line, likely indicative of the alignment of a channel at the time.

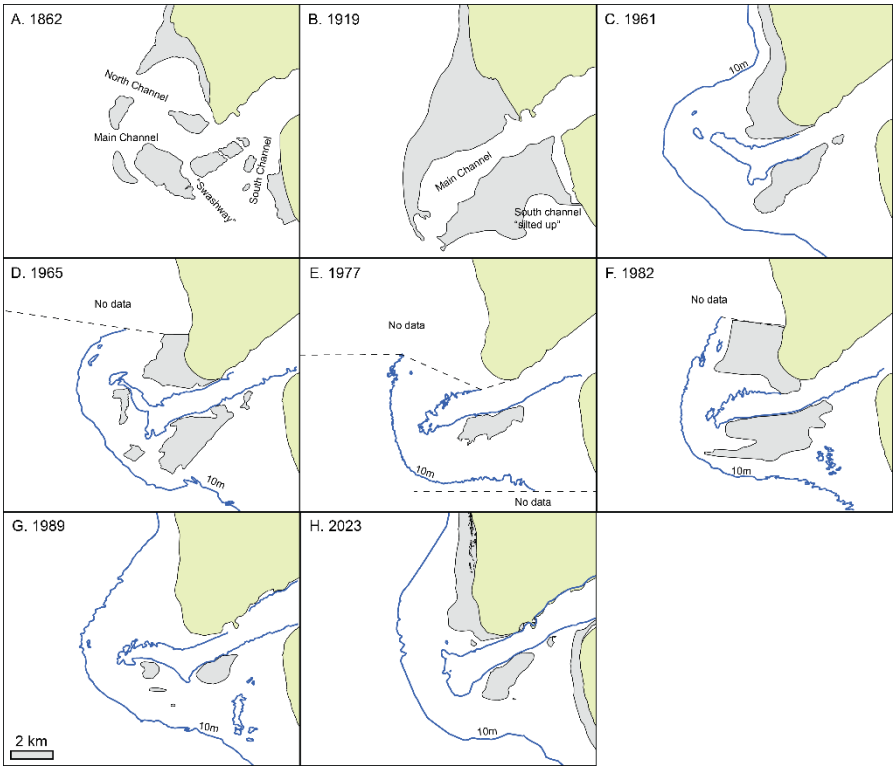

Figure 19. Channel and bar positions on the Manukau ebb-tidal delta interpreted from historic charts (1862 and 1919), survey sheets (1961-1989) and 2023 survey. The blue line indicates the position of the 6 fathom contour (10.97 m) (1961 and 1965) or 10 m contour (1977-2023). The bar positions are digitised from the outline of the bar as marked on the sheets, except for the 2023 survey where is it taken as the 3 m contour.

A defining feature of the METD in all charts and surveys is the “main bank”, “middle bank” or “south bank”, which is a channel margin linear bar (CMLB) or linear bar formation (LBF) on the southern flank of the main channel. The inner section of the bar is relatively stable across the surveys as indicated by the channel margin and the 10 m contour (Figure 20). Ford and Dickson (2018), along with satellite image analysis in this study (Figures 13 & 14), show the splitting of the south bank in 2015, which was likely the beginning of the process of a new, more southerly oriented channel being formed through the bifurcation of the bar. Similar bifurcation of the south bank is documented in the 1989 sounding sheets as well as the 1862, 1992 and 1999 charts, with evidence of the bifurcation of the bar absent in the 2004 chart.

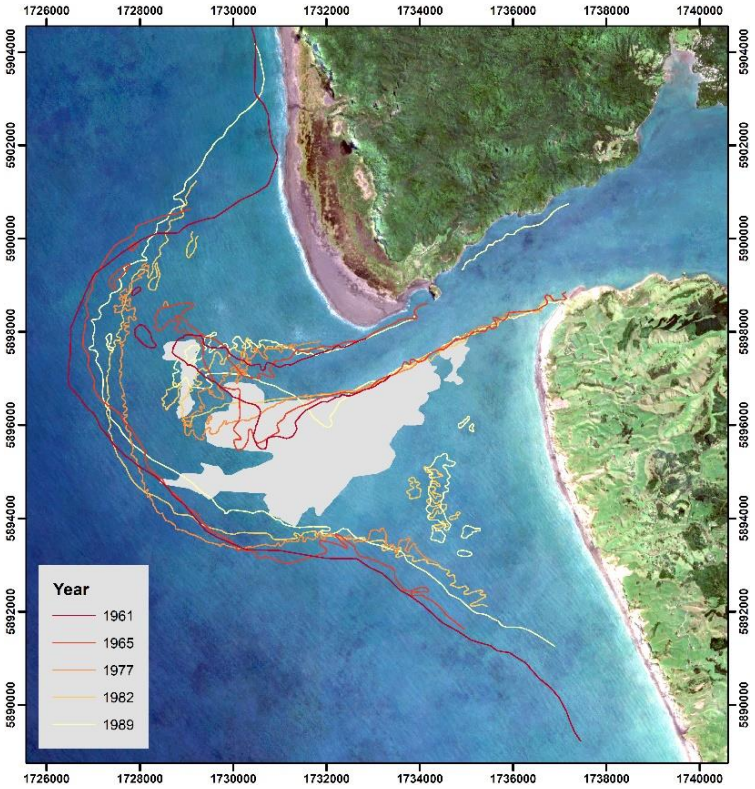

Figure 20. 10 m water depth contour and maximum extent of the south bank/bar (grey polygon) from sounding sheets. Note – depths and contours on the 1961 and 1965 sounding sheets are presented in fathoms, with the 6 fathom (10.97m) contour mapped as no 10 m contour is available.

4.3 Geomorphic changes of the METD from hydrographic surveys

4.3.1 1989 and 2023 surveys

The 1989 and 2023 Digital Elevation Models (DEM) generated from historic sounding sheets (1989) and survey completed for this study (2023), provide the only records which captures the morphology of the entire Manukau ebb-tidal delta system and surrounds (Figures 21 & 22).

Across the spatial extent of the clipped 1989 and 2023 DEMs there has been an average bed level change of -0.44 m (lowering), with values ranging between -13.34 m and 13.13 m (Figure 23). There are notable differences in the position of the bars and the orientation of the main channel between 1989 and 2023 (Figures 21 & 22). In 1989 the main channel was oriented in a westerly direction whereas in 2023 the channel was oriented in a west-southwest direction. Due to the more southerly orientation of the channel in 2023 there has been notable deposition of material to the north of the 2023 channel where the 1989 channel infilled. Bed level changes in this area are typically >5 m, with some areas characterised by >10 m of change. It is also evident that the terminal lobe is in a more landward position in 2023 relative to 1989, with bed level changes typically >5 m in this area.

Cut and fill analysis indicated there was 111 x 10^6 m^3 of cut (erosion) and 73 x 10^6 m^3 of fill (deposition), resulting in a net 38 x 10^6 m^3 reduction in the volume of the METD between 1989 and 2023. The planform area of cut was 48.18 km^2 and 37.71 km^2 of the METD characterised by a deposition (i.e. fill because of decreasing water depth).

Satellite observations of bar and channel migration suggest that the METD is dynamic over timescales considerably shorter than the 34-year interval between the 1989 and 2023 DEMs (Section 4.1 and Ford and Dickson, 2018). The periodic cycle of channel migration and bar breaching presented by Ford and Dickon (2018) indicates it is likely that the volumetric changes observed on the METD between 1989 and 2023 are an underestimate of the volume changes that would be observed if comparisons were made of the METD morphology at the end-stages of the cycle.

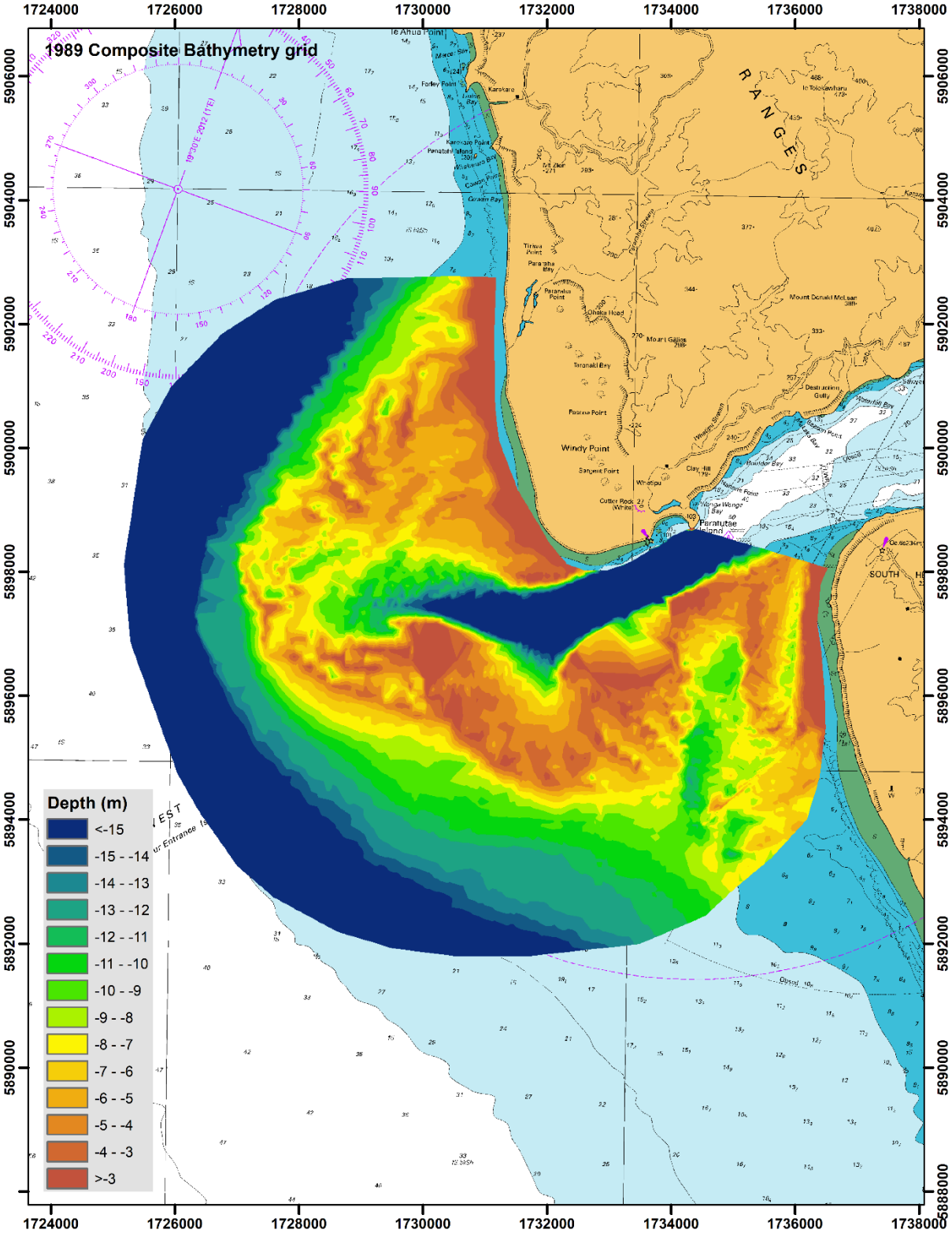

Figure 21. 1989 gridded bathymetry from digitised sounding sheets.

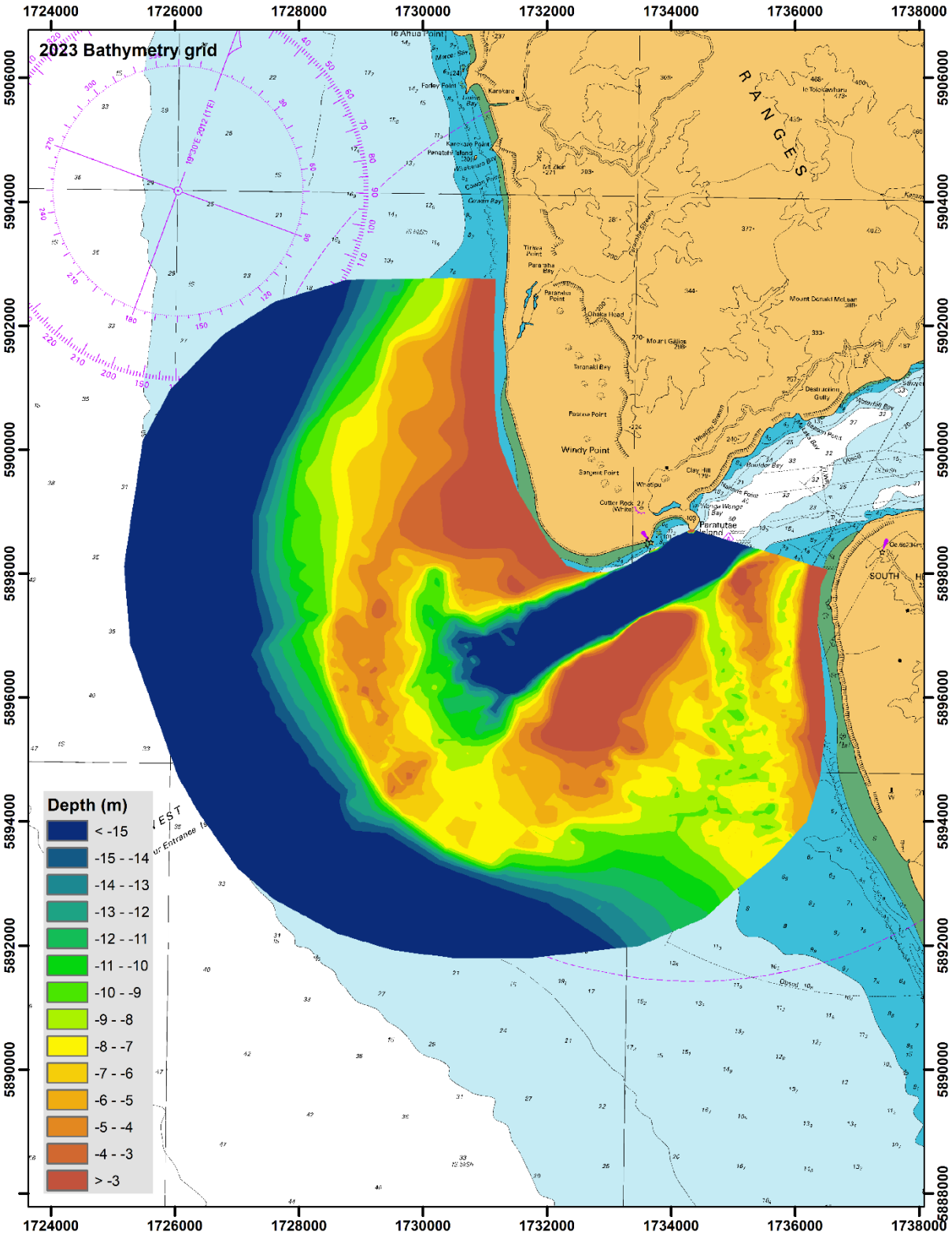

Figure 22. Gridded bathymetry from 2023 surveys.

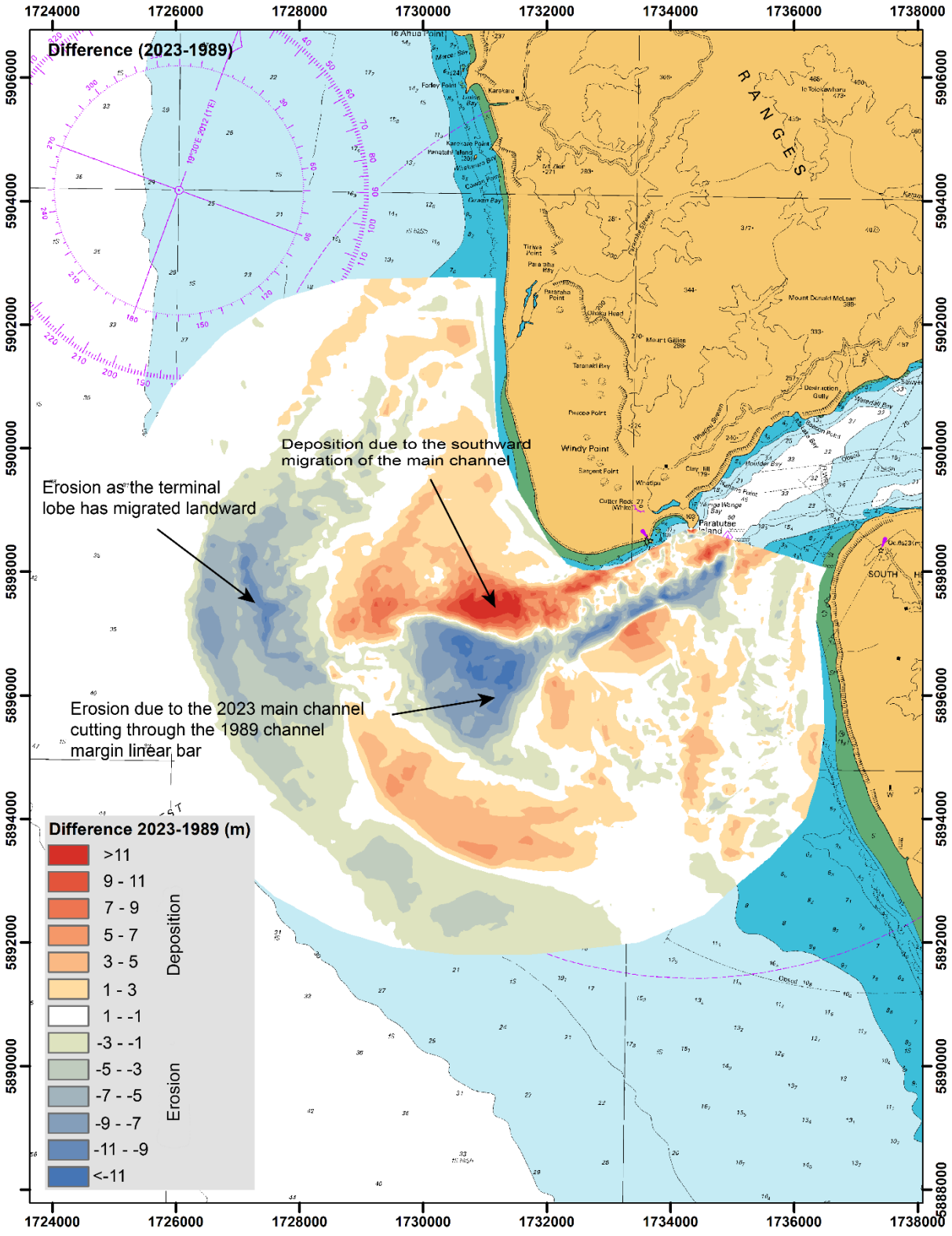

Figure 23. Difference between 1989 and 2023 bathymetry data.

4.3.2 Ports of the Auckland Surveys

The POAL dataset enables analysis of the bar and channel dynamics over shorter time periods than was possible using the 1989 and 2023 DEMs. Analysis of the POAL dataset involved both the point data (i.e. longitude, latitude, depth) and the DEMs generated from these data. In total, 40 DEMs from between 2001 and 2016 were generated and analysed. The October 2005 DEM was excluded from the analysis due to issues with the survey data which resulted in artefacts within the DEM. Of note, the spatial extent of each survey, and time period between surveys is unique, as a result, the volumes are not directly comparable through time. However, many surveys and the DEMs generated from these data have considerable spatial overlap with the preceding and following surveys which enables analysis of short-term changes.

In many areas the bed level changed by >2 m between surveys, with areas of both deposition and lowering of the bed level (i.e. erosion) evident in within the overlapping survey extent. Rather than uniform changes of bed level there are discrete areas of both erosion and deposition (Figure 24). The areas of the notable bed level change are likely the result of seabed features such as migrating bedforms. For example, Figure 24 presents the difference between the August 2014 and December 2014 surveys. It is evident that there are continuous, linear areas of deposition (i.e. decreased depth in December 2014 relative to August 2014). These are likely the result of large, subaqueous dunes, likely aligned perpendicular with tidal flow directions. Conversely, areas of erosion (i.e. increase depth in December 2014 relative to August 2014) likely indicate the migration of the bedform trough. Similar bedforms are evident within the repeated survey transects (Figure 25) and comparison of other DEMs (Appendix 3).

The volume of erosion (cut) between consecutive surveys ranged from 161,000 m^3 to 3,312,000 m^3 with an average of 1,037,000 m^3. The volume of deposition (fill) between consecutive surveys ranged between 145,000 m^3 and 2,238,000 m^3. The net volume change is the sum of areas of deposition and areas of erosion. The net volume change between surveys ranged from -2,923,000 m^3 and 1,913,000 m^3. The average net volume change was -489,000 m^3.

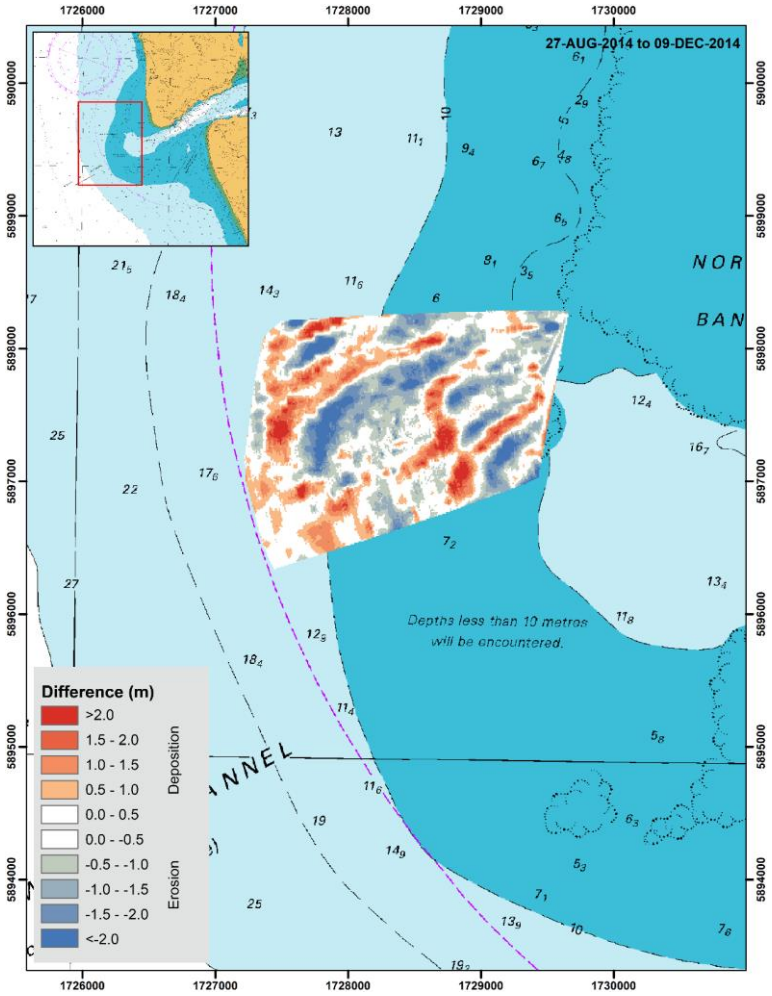

Figure 24. Difference between the Dec-2015 and Aug-2014 DEMs showing the presence of migrating bedforms.

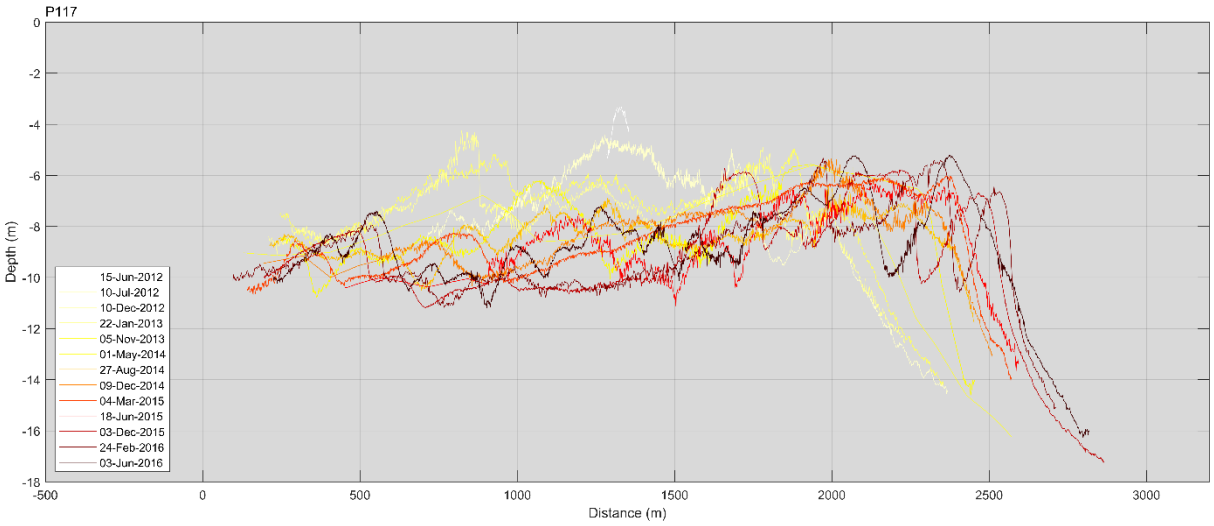

Figure 25. Along-channel profile (profile 117) from POAL surveys showing the migration of the terminal lobe (right hand side, ~2500 m distance) and bedform migration.

4.3.3 Cross channel changes

Analysis of the historic charts and the 1989 and 2023 surveys show the cycle of changes as the channel orientation switches between a more westerly and south-westerly orientation. The POAL surveys often revisited and surveyed four transects in the outer-section of the channel that are perpendicular to the along-channel transects (Figures 4 and 26). To further examine the channel changes, each of the four cross-channel profiles were split into the south and north side of the channel (Figure 27). Changes to the south side of the channel are assumed to represent the northward movement of sediment from the channel margin linear bar into the channel.

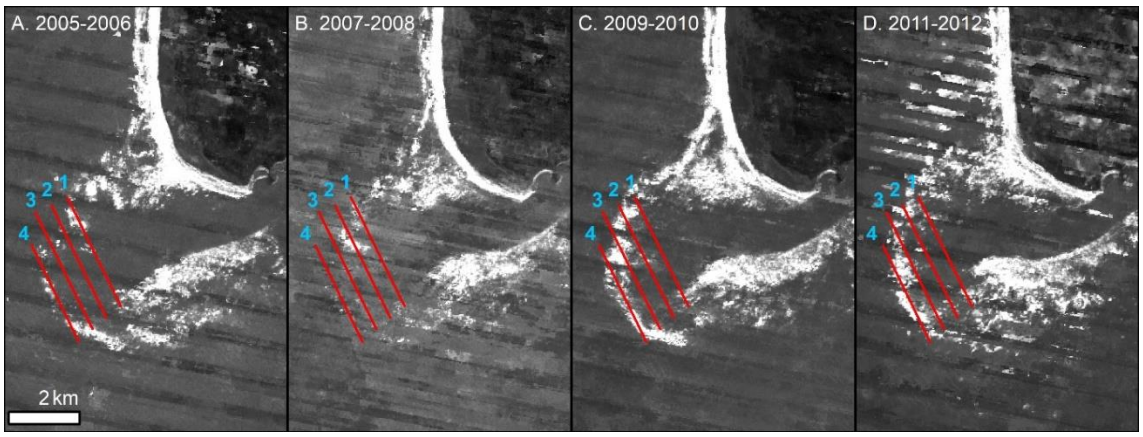

Figure 26. Location of cross-channel profiles surveyed by POAL overlaid time-averaged satellite imagery (see section X) of entrance to the Manukau Harbour.

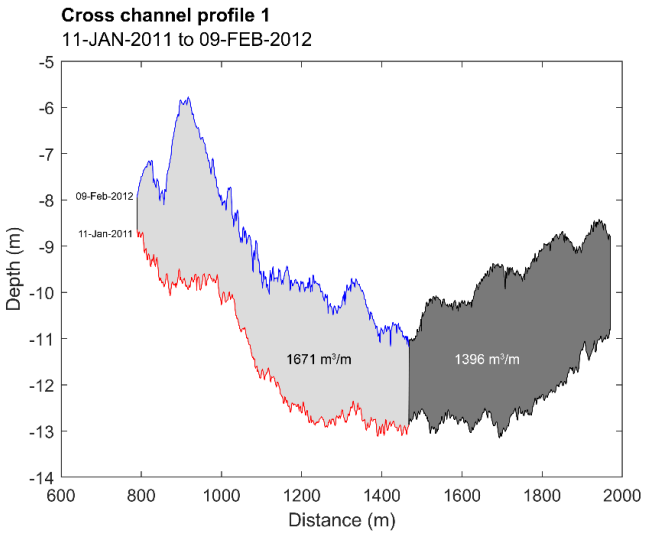

Figure 27. Example of cross-section area change of the main channel at cross-channel profile 1. The channel is split into the southern (left hand side) and northern section of the channel at the deepest point of the channel.

There is a notable decrease in the definition of the channel in a seaward direction from cross channel profile 1 to profile 4 (Figure 28). The channel is well-defined in cross-channel profile 1, with clear channel

edges. However, the channel edges at profiles 2-4 are low-slope and in some surveys, it is not possible to distinguish a channel. Surveys indicate that the south bank of the channel at profile 1 moved north ~800 m between 2005 and 2012, a rate of ~115 m/yr (Figure 28). This rate is broadly consistent with the estimated rate of 140 m/yr from satellite imagery (Section 4.1). The average cross-sectional area change of the southern half of the channel at profile 1 was 346 m^2 between surveys. This equates to rates ranging from -25 m^2/yr to 1548 m^2/yr, with an average rate of 529 m^2/yr. As a volume, this cross-sectional area change equates to 529 m^3/yr of change per linear meter of the channel. It is unknown how characteristic this rate of change would be along the entire southern bank of the channel as there are limited survey data in this area. However, satellite analysis (Figure 16) indicates the inner section (~2 km seaward of Paratūtai Island) of the channel appears stable, with areas further seaward of the inner section showing high levels of change due to the migration of the channel margin linear bar and the main channel. The area of the channel between 2 km seaward of Paratūtai Island and cross-channel profile 1 likely experiences similar changes as observed at cross-channel profile 1, however, it is only possible to observe these changes from satellite imagery and not possible to quantify volumetric changes using survey data.

Table 1. Cross-section area changes at cross-channel profile 1.

Date			Cross-sectional area change (m^2)			Rate (m^2/yr)		
First survey	Second survey	Duration (days)	Full channel	South side	North side	Full channel	South side	North side
1-Sep-05	16-Aug-06	349	1608.40	495.72	1112.68	1682.14	518.44	1163.70
16-Aug-06	24-Jan-07	161	39.90	-10.93	50.83	90.45	-24.77	115.23
24-Jan-07	29-Nov-07	309	-36.77	213.10	-249.87	-43.44	251.72	-295.15
11-Apr-08	7-Aug-08	118	-209.20	-22.33	-186.87	-647.09	-69.06	-578.03
7-Aug-08	3-Dec-08	118	-665.53	-85.74	-579.79	-2058.63	-265.22	-1793.41
3-Dec-08	4-Apr-09	122	70.81	146.04	-75.24	211.84	436.94	-225.10
4-Apr-09	27-Jul-09	114	-425.73	341.95	-767.68	-1363.08	1094.84	-2457.92
27-Jul-09	4-Feb-10	192	-1148.20	242.33	-1390.53	-2182.78	460.68	-2643.46
4-Feb-10	11-Jan-11	341	416.36	430.10	-13.74	445.66	460.37	-14.71
11-Jan-11	9-Feb-12	394	3067.00	1670.90	1396.10	2841.26	1547.91	1293.34
9-Feb-12	28-Apr-12	79	209.49	251.84	-42.35	967.91	1163.56	-195.65
28-Apr-12	10-Dec-12	226	443.47	478.89	-35.42	716.23	773.43	-57.20

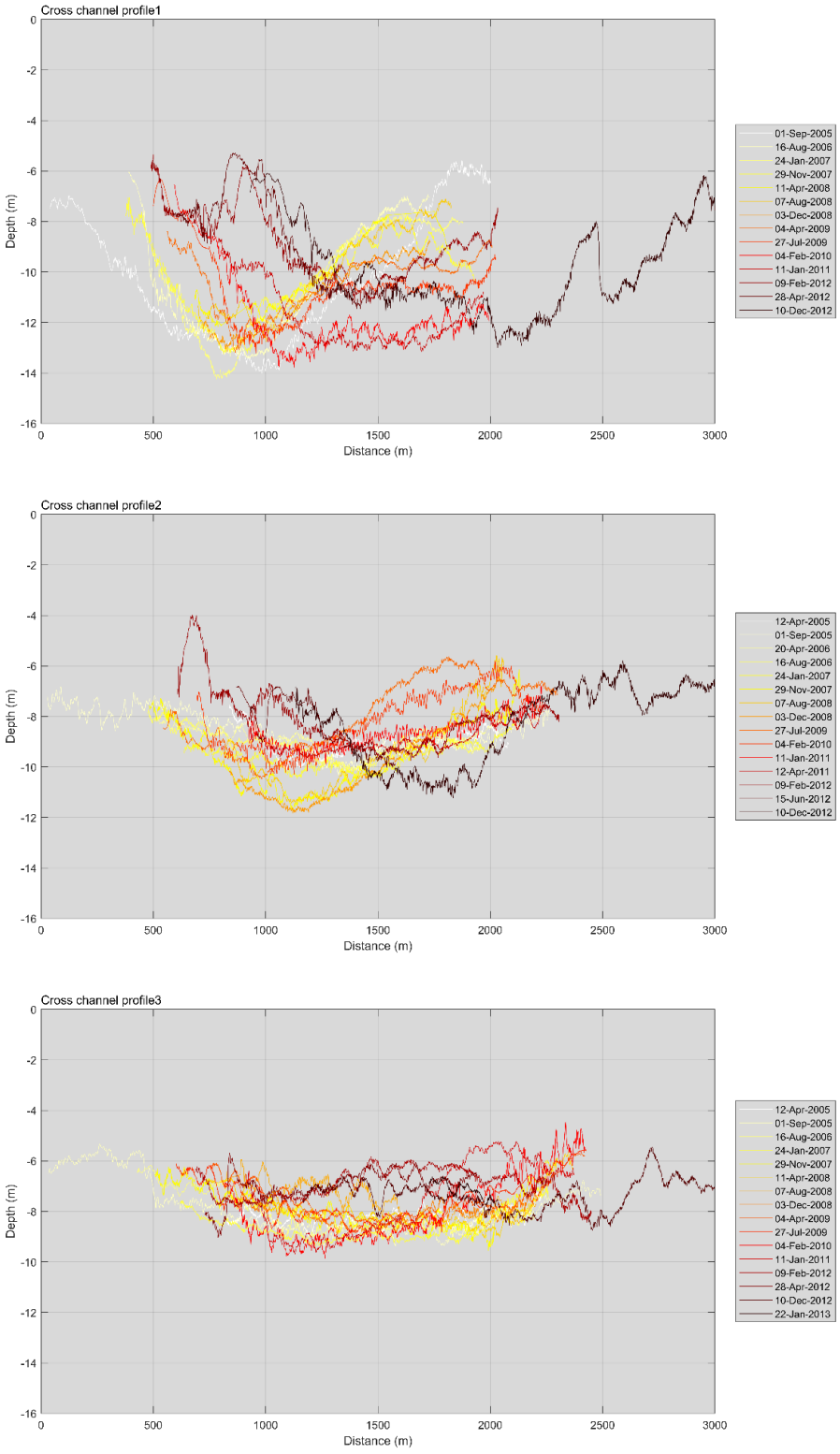

Figure 28. Cross-channel profiles 1-4 from POAL surveys.

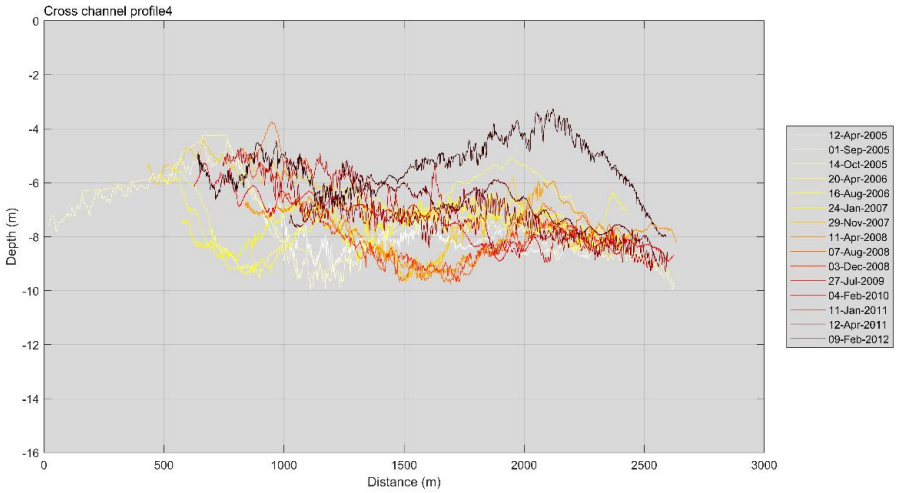

Figure 28 continued. Cross-channel profiles 1-4 from POAL surveys.

5 INTERPRETATON OF BAR AND CHANNEL DYNAMICS

Collectively, information from historic navigation charts, hydrographic surveys and the analysis of optical satellite imagery show the METD exhibits a complex array of large-scale geomorphic changes which are characteristic of ebb-tidal deltas. FitzGerald (1988) proposed a conceptual model of ebb-tidal delta dynamics, which was later expanded upon by FitzGerald et al. (2000) (Figure 29). This model outlined five potential sequences of behaviour of ebb-tidal deltas, along with a sixth stable form. Ford and Dickson (2018) noted several similarities between the behaviour of the METD and the *Ebb-tidal delta breaching* and *Outer channel shifting* behaviours described by FitzGerald et al. (2000) (Figure 30). Ford and Dickson (2018) observed a new channel, which seems to have branched off from the northern channel in 2015-2016, displaying a roughly north-south orientation. This behaviour aligns with the *Ebb-tidal delta breaching* proposed by FitzGerald et al. (2000), wherein a new, more direct seaward channel emerges, diverting a significant portion of the ebb-tidal flow and eventually leading to the closure of the previous channel.

All historic and recent survey data indicate there are noteworthy changes in bed level and volume resulting from shift in the position of the main channel and the channel margin linear bar, terminal lobe and other sand bars. Collectively the geomorphic changes within the METD system are a product of changes over different spatial and temporal scales. For example, the complete cycle of ebb-tidal delta breaching appears multi-decadal, potentially operating on an ~20 year cycle. Conversely, high levels of change occur over sub-annual timescales, with the migration of the large bedforms (Figure 24) and deposition of sediment resulting from the northward movement into the channel (Figure 28). It is likely that sediment transport on the event, tidal and seasonal timescales also likely drive geomorphic changes to the METD but are unable to be quantified using the survey or satellite data available.

The large-scale geomorphic behaviour of the METD is dominated by the cyclical behaviour of the system, which approximates the *Ebb-tidal delta breaching* process. This process results in massive redistribution of sediment as the main channel oscillates between westerly and south-westerly orientations. Comparison of the 1989 and 2023 surveys, neither of which are likely to have captured the end states of *Ebb-tidal delta breaching* process, indicate that over this period there was 111 x 10^6 m^3 of cut (erosion) and 73 x 10^6 m^3 of fill (deposition) of material, resulting in a net reduction of 38 x 10^6 m^3 of the volume of the METD between 1989 and 2023. The observations of large-scale geomorphic changes were also evident within the satellite record which showed 1-2 km changes in the position of the terminal lobe (Figure 15) as well as in the position of the channel margin linear bar and main channel (Figure 16).

Geomorphic changes over sub-annual time periods was assessed using the POAL surveys. These data reveal two notable mechanisms driving changes in the geomorphology of the METD. First, observations of large, highly mobile bedforms is evident from both the point and gridded POAL data (Figures 24 and 25). Bedforms were observed to drive changes of >2 m in bed level over ~3 months (Figure 24). Second, the southern bank of the outer section of the main channel was observed to have moved northward by ~800 m between 2005 and 2012 (Figures 16 and 28). This northward shift of the channel resulted in volume of change at cross-channel profile 1 estimated at 529 m^3 per linear meter of channel (Table 1.). The observations of northward migration of the main channel evident from the analysis of the POAL data was also evident within the satellite record which showed notable northward movement of the southern margin of the channel (Figure 16). Collectively, the analysis and interpretation of the bathymetric datasets and satellite record reveal the complexity of the process of geomorphic changes on the METD over centennial, decadal and sub-annual timescales which are consistent with observed and modelled behaviours of other similar systems.

Dastgheib (2012) used a numerical model to examine the morphological evolution of an inlet system based on the Ameland tidal basin in Dutch Wadden Sea. In wave dominated model runs (Hs 2.1 m, tidal range 0.86 m) Dastgheib (2012) observed ebb-tidal delta breaching with the cycle occurring over a 15–20-year period and noted that when the volume of sediment in the ebb-tidal delta is larger, this cycle takes longer. Of note, Dastgheib (2012) also observed that in model runs with a greater tidal range (Hs 2.1 m, tidal range 1.72 m), closer to the conditions at the METD, that similar ebb-tidal delta breaching was observed. However, Dastgheib (2012) noted the cyclic channel migration is limited to the outer part of the channel while the inner part remains stable. This behaviour, and the timescales over which it occurs, are similar to what was seen in the historic charts and surveys as well as the analysis of satellite imagery of the METD.

Similarly, Lenstra et al. (2019) used numerical models (SWAN and Delft3D) to model cyclical behaviour of ebb-tidal delta, focussing on *Ebb-tidal delta breaching* and *Outer delta breaching* processes. The behaviour of the modelled ETD in Lenstra et al., (2019) resembled the conceptual behaviour suggested by FitzGerald et al. (2000) and that observed on the Manukau Harbour ebb-tidal delta and other similar sites globally. Lenstra et al., (2019) noted this behaviour is governed by the ratio of tidal prism (Mm^3) to littoral drift (Mm^3), with this ratio providing an indication as whether the ETD would be characterised by *Ebb-tidal delta breaching*, *Outer delta breaching* or *Stable inlet processes*.

By extending the period of analysis from satellite imagery to 2022 it is increasingly evident the METD adheres to the *Ebb-tidal delta breaching* model proposed by FitzGerald et al. (2000) (Figure 29) and

adapted for the METD by Ford and Dickson (2018) (Figure 30). The period of this cycle appears ~20 years, with the time-averaged image from 1999-2000 appearing in somewhat similar as the 2021 image, with images in the years between showing evidence of the cyclical process of *Ebb-tidal delta breaching*. Similarly, the historic charts provide evidence of this cycle, but given the irregular sampling it is not possible to determine whether this cycle operated over the period prior to the satellite imagery record.

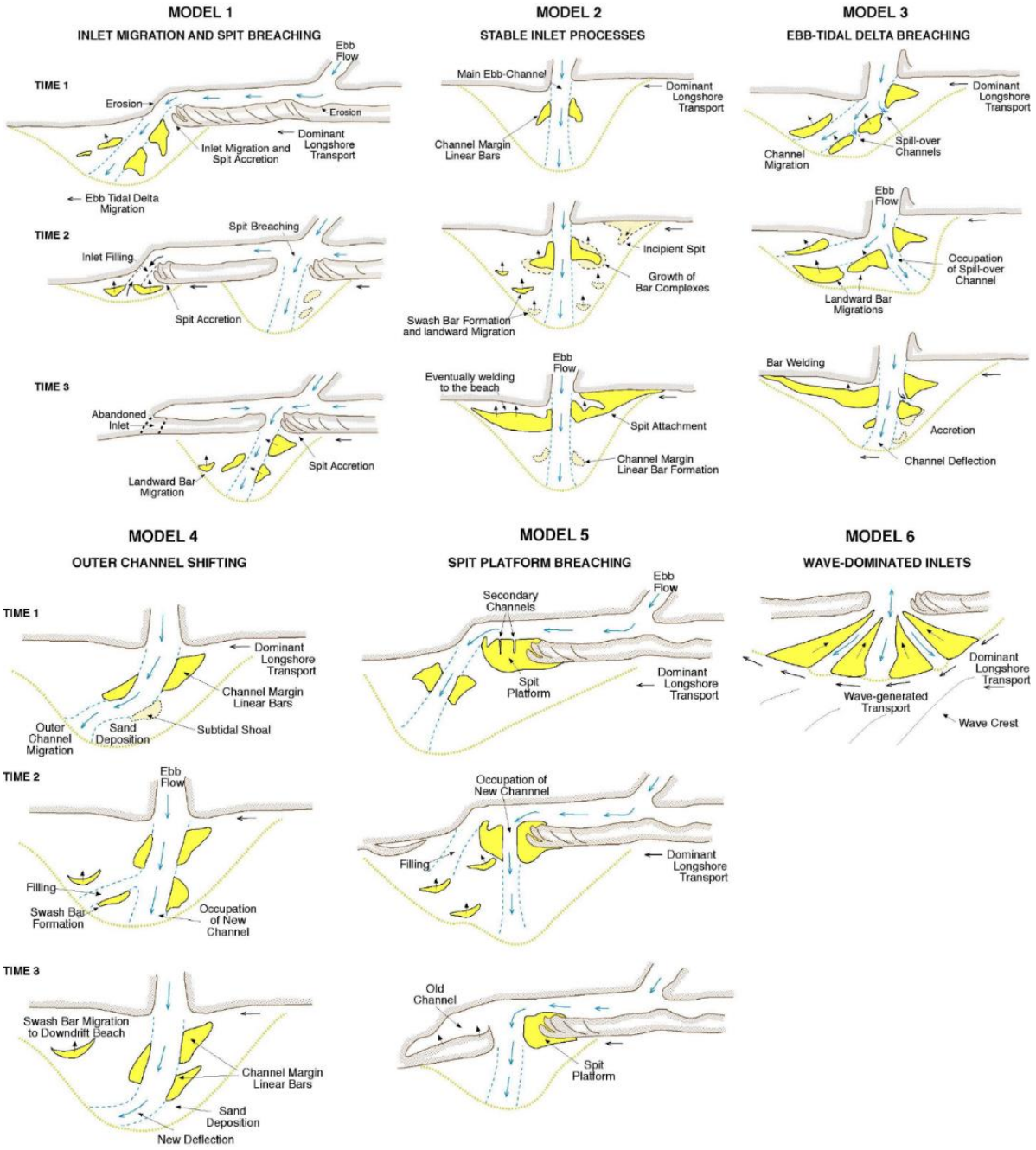

Figure 29. Conceptual model of ebb-tidal delta dynamics proposed by FitzGerald et al. (2000).

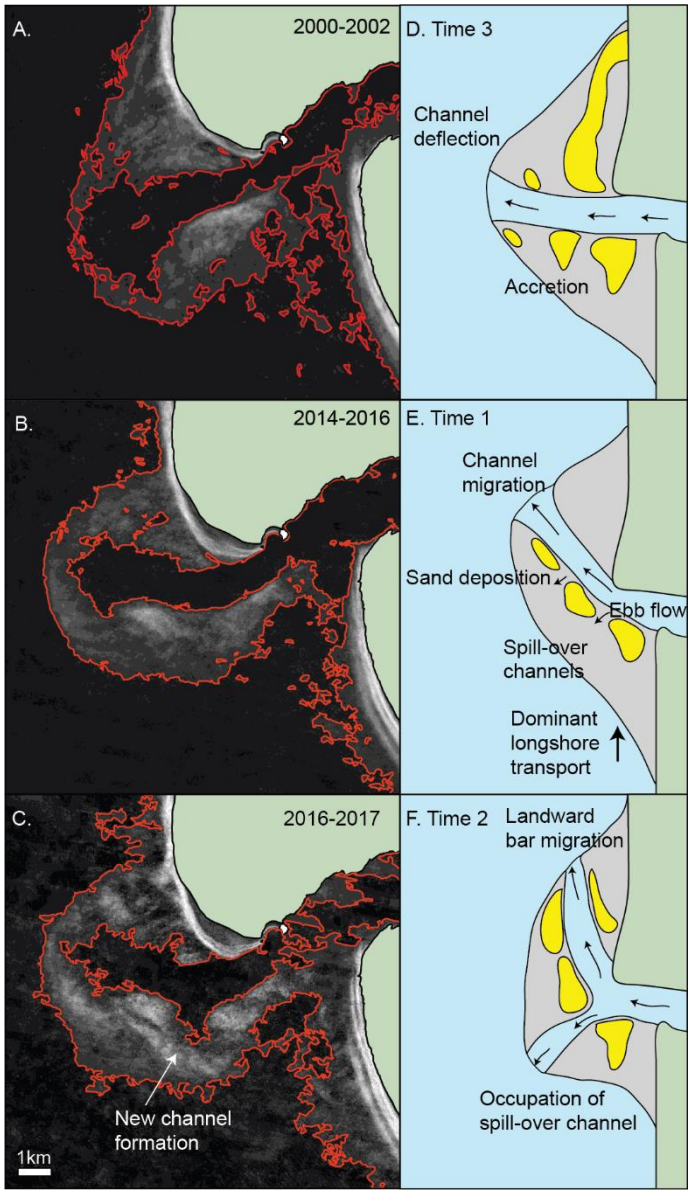

Figure 30. Conceptual model of METD dynamics developed by Ford and Dickson (2018) based on FitzGerald et al. (2000)

6 REFERENCES CITED

Cowan, J., Pomare, S. M., & Peterson, S. (1930). *Legends of the Maori: Mythology, Folk-Lore, Tradition and Poetry* Fine Arts.

Dastgheib, A. (2012). Long-term process-based morphological modeling of large tidal basins. PhD thesis UNESCO-IHE/DUT

Durrant, Thomas; Hemer, Mark; Trenham, Claire; Greenslade, Diana (2013): CAWCR Wave Hindcast 1979-2010. v10. CSIRO. Service Collection. http://hdl.handle.net/102.100.100/13165?index=1

EL-Hattab, A. I. (2014). Single beam bathymetric data modelling techniques for accurate maintenance dredging. *The Egyptian Journal of Remote Sensing and Space Science, 17*(2), 189-195.

FitzGerald, D. M. (1984). Interactions between the ebb-tidal delta and landward shoreline; Price Inlet, South Carolina. *Journal of Sedimentary Research, 54*(4), 1303-1318.

FitzGerald, D. M., Kraus, N. C., & Hands, E. B. (2000). Natural mechanisms of sediment bypassing at tidal inlets.

Ford, M. R., & Dickson, M. E. (2018). Detecting ebb-tidal delta migration using Landsat imagery. *Marine Geology, 405*, 38-46.

Ford, M., & Dickson, M. (2019). The use of Planet cubesat imagery to examine ebb-tidal delta dynamics. In *Coastal Sediments 2019: Proceedings of the 9th International Conference* (pp. 2500-2510).

Ford, M. R., Dickson, M. E., & Durrant, T. H. (2021). Mapping ebb tidal delta dynamics using Planet cubesat imagery within the Google Earth Engine. In *Australasian Coasts & Ports 2021: Te Oranga Takutai, Adapt and Thrive: Te Oranga Takutai, Adapt and Thrive* (pp. 424-428). Christchurch, NZ: New Zealand Coastal Society.

Gorelick, N., Hancher, M., Dixon, M., Ilyushchenko, S., Thau, D., & Moore, R. (2017). Google Earth Engine: Planetary-scale geospatial analysis for everyone. *Remote Sensing of Environment,* doi://doi.org/10.1016/j.rse.2017.06.031

Harrison, S. R., Bryan, K. R., & Mullarney, J. C. (2017). Observations of morphological change at an ebb-tidal delta. *Marine Geology,* doi://doi.org/10.1016/j.margeo.2016.12.010

Hayes, M. O. (1980). General morphology and sediment patterns in tidal inlets. *Sedimentary Geology, 26*(1-3), 139-156.

Hayes, M. O., & FitzGerald, D. M. (2013). Origin, evolution, and classification of tidal inlets. *Journal of Coastal Research,* (69 (10069)), 14-33.

Hicks, D. M., & Hume, T. M. (1996). Morphology and size of ebb tidal deltas at natural inlets on open-sea and pocket-bay coasts, North Island, New Zealand. *Journal of Coastal Research*, 47-63.

Hicks, D. M., & Hume, T. M. (1997). Determining sand volumes and bathymetric change on an ebb-tidal delta. *Journal of Coastal Research,* 407-416.

Holdaway, A., Ford, M., & Owen, S. (2021). Global-scale changes in the area of atoll islands during the 21st century. *Anthropocene, 33*, 100282.

Lenstra, K. J., Ridderinkhof, W., & van der Vegt, M. (2019). Unraveling the Mechanisms That Cause Cyclic Channel-Shoal Dynamics of Ebb-Tidal Deltas: A Numerical Modeling Study. *Journal of Geophysical Research: Earth Surface, 124*(12), 2778-2797.

Markham, B. L., Storey, J. C., Williams, D. L., & Irons, J. R. (2004). Landsat sensor performance: history and current status. *IEEE Transactions on Geoscience and Remote Sensing, 42*(12), 2691-2694.

Scaramuzza, P., Micijevic, E., & Chander, G. (2004). SLC gap-filled products phase one methodology. *Landsat Technical Notes, 5*

Walton Jr, T. L., & Adams, W. D. (1976). Capacity of inlet outer bars to store sand. *Coastal Engineering 1976* (pp. 1919-1937)